Journal of Volcanology and Geothermal Research, 58 (1993) 101–132
Elsevier Science Publishers B.V., Amsterdam

Modeling of the ascent of magma during the plinian eruption of Vesuvius in A.D. 79

Paolo Papale[a,b] and Flavio Dobran[b,c]
[a]*GNV, Università di Pisa, Via S. Maria 53, 56100 Pisa, Italy*
[b]*Istituto Nazionale di Geofisica, Roma, Italy*
[c]*Department of Earth System Science, New York University, New York, NY 10003, USA*

(Received February 13, 1992; revised version accepted September 8, 1992)

ABSTRACT

The ascent of magma during the A.D. 79 eruption of Vesuvius was studied by a steady-state, one-dimensional, and nonequilibrium two-phase flow model. The gas exsolution process was modeled by assuming a chemical equilibrium between the exsolved and dissolved gas, whereas the magma density and viscosity were modeled by accounting for the crystal content in magma. The exsolution, density, and viscosity models consider the effect of different compositions of the white and gray magmas. By specifying the conduit geometry and magma composition, and employing the model to search for the maximum discharge rate of magma which is consistent with the specified geometry and magma composition, the model was then used to establish the two-phase flow parameters along the conduit. It was found that for all considered conditions the magma pressure in the conduit decreases below the lithostatic pressure near the magma fragmentation level, and that in the deep regions of the conduit the white magma pressure is larger and the gray magma pressure is lower than the lithostatic one. The exsolution and fragmentation levels were found to be deeper for the white than for the gray magma, and the changing composition during the eruption causes an increase of the exit pressure and decrease of the exit gas volumetric fraction. The model also predicted a minimum conduit diameter which is consistent with the white and gray magma compositions and mass flow-rates. The predictions of the model were shown to be consistent with column collapses during the gray eruption phase, large presence of carbonate lithics in the gray pumice fall deposit, and magma–water interaction during a late stage of the eruption.

1. Introduction

Vesuvius is the most dangerous and famous of all volcanoes. During its long history it produced different kinds of volcanic activities, ranging from an effusive behavior to very violent explosive eruptions. At least seven eruptions in the last 17,000 years have been explosive plinian-type eruptions (Santacroce, 1987), where each was preceded by a long period of quiescence during which the differentiation processes within the magma chamber produced a water-rich phonolitic or tephritic-phonolitic magma (Barberi et al., 1981). The high viscosity and dissolved water contents of these magmas were responsible for the high explosivity of the eruptions.

In spite of a great deal of accumulated knowledge, the Vesuvius continues to be a formidable menace to its neighbouring populations. This is true today more than at any time in the past, because of the continuing urbanization below its flanks. The A.D. 79 eruption of Vesuvius stands as a reminder of its destructiveness, both in property and human toll. The eruption started at about 1 p.m. on August 24 with the formation of a plinian column that was preceded by a phreatomagmatic opening phase. For the following seven hours, a phonolitic magma (white pumice) was erupted and the magma discharge rate increased from about 5×10^6 to 8×10^7 kg/s. At about 8 p.m. on the same day, the magma composition changed to tephritic phonolite (gray pumice) and the dis-

0377-0273/93/$06.00
SSDI 0377-0273(93)E0021-S

charge rate reached a maximum value of 1.5×10^8 kg/s at 1 a.m. on August 25. After this time, several pyroclastic surges occurred, the first of which destroyed Herculaneum and the fourth of which destroyed Pompei and killed about 2000 people (Sigurdsson et al., 1985, 1990; Carey and Sigurdsson, 1987). During the pyroclastic surge emplacement the plinian column was sustained to produce intermingled surge and pumice fall deposits. The variation of magma composition during the eruption can be associated with a compositionally zoned magma chamber, where an evolved and volatile-rich white magma overlied a more mafic and less volatile-rich gray magma (Barberi et al., 1981; Cornell and Sigurdsson, 1987; Sigurdsson et al., 1990; Civetta et al., 1991).

The explosive eruptions are characterized by very high magma viscosities, and very few attempts have been made in the past to model the flows of such magmas through the volcanic conduits (Dobran, 1992). Recently, Dobran (1992) applied a nonequilibrium two-phase flow model to the magma flow in the volcanic conduits of Mt. St. Helens on May 18, 1980, and Vesuvius in A.D. 79 and found that the large magma viscosities can produce large differences between the lithostatic and magma pressures near the magma fragmentation zone, and large nonequilibrium effects between the phases after the magma fragments. In this modeling it was assumed that the liquid magma density is constant and that the viscosity can be calculated from an empirical expression, without accounting for the composition of magma.

The objectives of the present work are: (1) to employ the nonequilibrium two-phase flow model of Dobran (1992) for magma flow through the conduit of Vesuvius during its eruption in A.D. 79; (2) to incorporate into the model compositionally dependent magma density, gas exsolution, and viscosity models; and (3) to infer new information on the flow dynamics of magma ascent in the conduit and on the eruption parameters, such as conduit diameter, and exit pressure and velocities of gas and fragmented magma. The input data to the model, consisting of the magma discharge rate, conduit geometry, stratigraphy of rocks surrounding the conduit, and magma composition, were determined on the basis of a large number of petrological and volcanological studies of Vesuvius. With the changing magma composition from white to gray, the model predictions are consistent with an increase of the deep lithic content in the deposits, increasing conduit diameter, a larger possibility of column collapses during the gray pumice eruption phase, and a late stage magma–water interaction.

2. Products of the plinian eruption of Vesuvius in A.D. 79

As discussed above, the plinian fall deposit of the A.D. 79 eruption of Vesuvius is characterized by a vertical compositional variation from phonolite at the bottom to tephritic phonolite at the top. This feature is marked in the field by a sudden change in the overall color of the deposit, being white in its lower portion (the white pumice) and gray in the upper portion (the gray pumice) (Lirer et al., 1973; Barberi et al., 1981; Sheridan et al., 1981; Sigurdsson et al., 1982, 1985, 1990; Carey and Sigurdsson, 1987). This appearance, which is not accompanied by any indication of a depositional break, is the result of both higher iron and titanium contents in the residual liquid and higher abundance of mafic microlites in the gray pumice with respect to the white pumice (Barberi et al., 1981). The vertical chemical variation is not continuous, but it is characterized by a compositional gap which appears to reflect the existence of a compositionally zoned magma chamber (Cornell and Sigurdsson, 1987; Sigurdsson et al., 1990; Civetta et al., 1991). The chemical analyses of the mechanically separated glass portion of the white and gray pumice are given by Barberi et al. (1981) and are reproduced in Table 1 normalized to

TABLE 1

Anhydrous chemical composition of the AD 79 white and gray magmas (after Barberi et al., 1981)

	SiO_2	TiO_2	Al_2O_3	Fe_2O_3	FeO	MnO	MgO	CaO	Na_2O	K_2O	P_2O_5
White	56.39	0.22	22.06	1.46	0.90	0.11	0.15	2.67	7.35	8.67	0.02
Gray	54.98	0.54	20.21	2.67	1.84	0.12	1.48	4.86	4.98	8.14	0.18

100 without water. We assume that these analyses represent the anhydrous composition of the liquid magmas prior to the eruption. Because of the existence of a syn-eruptive mixing between the white and gray magmas, as demonstrated by Sigurdsson et al. (1990) on the basis of the mineralogy of the two types of pumice and of the distribution of minor elements, and by Civetta et al. (1991) on the basis of isotopic distribution, the above assumption is not strictly justified. However, with the exception of a restricted zone near the stratigraphic boundary between the white and the gray pumice, the amount of mixing does not exceed 20% (Sigurdsson et al., 1990). These analyses constituted the calculational basis of the compositionally dependent quantities, such as water solubility, density and viscosity of magma, which were computed as discussed in the following section.

Some other differences between the white and gray pumice are: (1) the gray pumice is more porphyritic than the white pumice and contains a larger amount of volcanic and metamorphic xenoliths; (2) the gray pumice is more coarse-grained than the white pumice in the same stratigraphic section as a consequence of an increase in the mass discharge rate of magma during the eruption (Carey and Sigurdsson, 1987; Sigurdsson et al., 1990); and (3) towards the top the gray pumice is interbedded with at least four finer coarse-ash layers whose origin has been a subject of different interpretations.

The finer ash layers are considered by Sheridan et al. (1981) to have formed during an early phase of explosive interaction of magma with ground water on the basis of their high fragmentation and the presence of sandwave bed forms. They explain the absence of "wet" characteristics in the deposit in terms of a small quantity of water interacting with magma which essentially vaporized the water into a superheated steam (Sheridan and Wohletz, 1983) and thus formed a "dry" pyroclastic surge. Sigurdsson et al. (1985) interpret, however, the finer ash layers as due to partial collapses of the plinian column without the intervention of external water and restrict the phreatomagmatic phase to the very final stages of the eruption where the deposit contains pisolites. Recently, Barberi et al. (1989) examined systematically many samples from vertical stratigraphic sequences of some eruptions of Vesuvius, including that of A.D. 79, and on the basis of the distribution of components among different grain size classes concluded that the interaction of magma with groundwater took place after the emplacement of the pumice flow which directly overlies the gray pumice. Therefore, following Barberi et al. (1989) and Civetta et al. (1991), four main phases of the A.D. 79 eruption can be distinguished:

(1) a phreatomagmatic explosive opening marked by an initial thin coarse-ash layer;

(2) a plinian phase which includes a fallout-derived white and gray pumice and the interbedded pyroclastic surges;

(3) a "dry surge and flow" phase which is mainly characterized by the collapse of the eruptive column; and

(4) a final "wet surge and flow" phase which groups all products with a phreatomagmatic origin.

In the present work, however, only the plinian

phase is being considered, since the magma–water interaction modeling has not been carried out satisfactorily to date (Dobran et al., 1990).

3. Magma flow modeling in volcanic conduit

3.1. Fluid dynamic modeling

The modeling of magma ascent during the plinian eruption of Vesuvius in A.D. 79 can be accomplished by the two-phase flow nonequilibrium model of Dobran (1992). This model describes the quasi-steady and one-dimensional flow of magma from the stagnation state o in the magma chamber through a conduit of length L (Fig. 1). The magma flow in a conduit leads to pressure decrease and exsolution of the dissolved magmatic gas. Beyond the exsolution point in a conduit at $z=z_s$ in Figure 1, the exsolved gas and magma flow as a two-phase bubbly mixture. As the bubbles in magma grow by gas diffusion and decompression, they eventually contribute to the magma fragmentation when their size and density

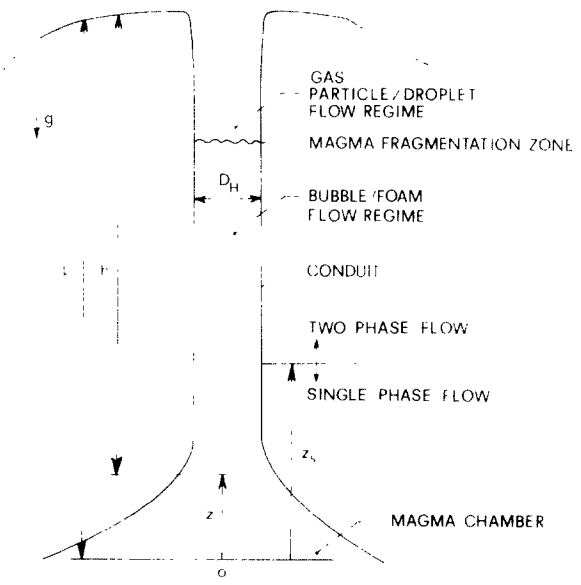

Fig. 1. Illustration of a volcanic conduit. The magma is accelerated from the stagnation state o in magma chamber and begins exsolving at $z=z_s$.

reach a maximum bubble packing limit. This limit appears to be well defined by the gas volumetric fraction of about 0.75 (Sparks, 1978; Dobran, 1992). After the magma fragments, the two-phase flow regime changes from a bubbly flow with bubbles dispersed in magma to a gas-droplet/particle flow with liquid magma drops or solid particles dispersed in a continuous gas phase. The transport of magma in the conduit is assumed to be isothermal but not in velocity equilibrium in the two-phase flow regimes. In the region from $z=0$ to $z=z_s$ the magma flow can be considered as an effective single phase fluid with a mean density and viscosity that account for the dissolved gas and crystals in the liquid. The single phase flow length z_s is established by applying a one-dimensional form of the momentum equation between the stagnation state o in the magma chamber and the height z_s, i.e.:

$$P_0 = P_s + (1+K)\frac{G^2}{2\rho_L} + 4z_s \frac{f_F}{D_H}\frac{G^2}{2\rho_L} + \rho_L g z_s \tag{1}$$

where P is the pressure, ρ_L is the effective density of magma, G is the mass flow-rate of magma per unit area, f_F is a friction loss coefficient, and D_H is the hydraulic diameter of the conduit which is defined in terms of the flow cross-sectional area A and wetted perimeter ξ. Thus:

$$D_H = \frac{4A}{\xi} \tag{2}$$

In Eqn. (1) K is the entrance loss coefficient, whereas the friction coefficient f_F depends on the Reynolds number and is given by:

$$f_F = \frac{B_1}{Re} + B_2, \quad Re = \frac{GD_H}{\eta_L} \tag{3}$$

where η_L is the magma viscosity and for circular conduits $B_1=16$ and $B_2=0.01$ (Dobran, 1992). The magma chamber pressure P_0 is bracketed by the lithostatic pressure of the overlying rocks and soil and the rock yield stress. However, in evaluating this pressure, use

will only be made of the actual stratigraphy of Vesuvius, since the yield stress of rocks at magma chamber depths is not known. Thus:

$$P_o = \int_0^L \rho_c g \, dz + P_{atm} \quad (4)$$

where ρ_c is the local density of the country rock which has a stratigraphic distribution as obtained by the geothermal well TRECASE-1 (Balducci et al., 1985). It should be noted, however, that these drilling data pertain to a stratigraphic section which is 2400 m removed from the caldera rim and 300 m below it. In our calculations of the A.D. 79 eruption we assumed the same stratigraphy and added 300 m of rocks with the same characteristics as the most superficial rocks of the drilling site (Fig. 2). Below about 2200 m to the magma chamber depth it was assumed that the stratigraphy is made up of carbonatic rocks. In the two-phase flow region $z > z_s$ (see Fig. 1) the flow is modeled by the following equations which express the conservation of mass and balance of momentum of gas and liquid (Dobran, 1992):

$$M_G = \rho_G \alpha A u_G = XM \quad (5)$$

$$M_L = \rho_L (1-\alpha) A u_L = (1-X)M \quad (6)$$

$$\rho_G u_G A \alpha \frac{du_G}{dz} = -\alpha A \frac{dP}{dz} - F_{LG}A - F_{wG}A - \rho_G g \alpha A \quad (7)$$

$$\rho_L u_L A (1-\alpha) \frac{du_L}{dz} = -(1-\alpha)A \frac{dP}{dz} + F_{LG}A - F_{wL}A - \rho_L g (1-\alpha) A \quad (8)$$

where M is the magma mass flow-rate, u is the velocity, α is the gas volumetric fraction, X is the exsolved gas mass fraction, and where the subscripts G and L pertain to the gas and liquid, respectively. In the above equations the gas component is water vapor and the liquid is magma before magma fragments and liquid drops or particles after magma fragments (Fig. 1). The density of liquid ρ_L accounts for the composition of magma and crystal content and is allowed to change due to the gas exsolution.

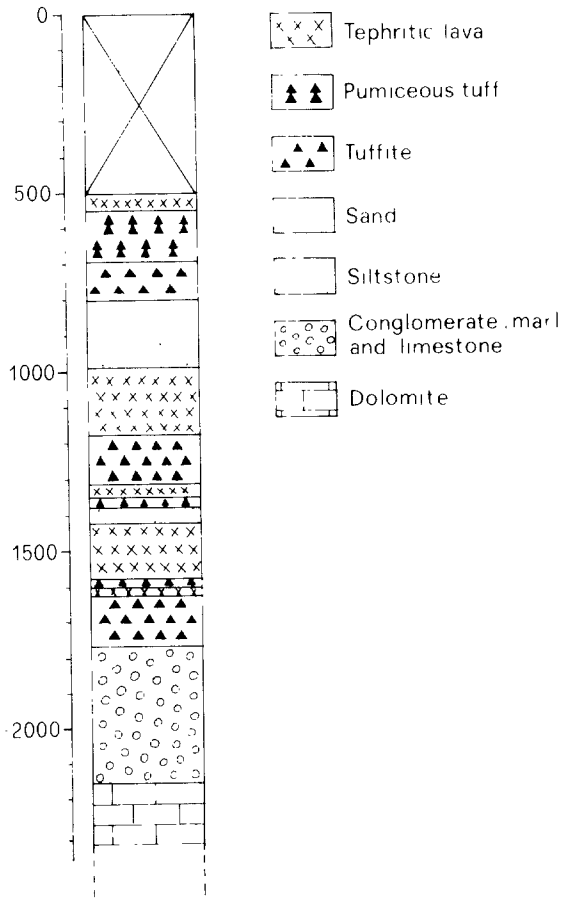

Fig. 2. Assumed stratigraphy of the surrounding conduit rocks in the model. This is a modified stratigraphy pertaining to the TRECASE-I well (Balducci et al., 1985) drilled about 2 km from Somma-Vesuvius caldera rim. The first superficial 500 meters correspond to recent volcanic deposits and to lavas and pyroclastites of the Somma-Vesuvius. The carbonatic rocks were assumed to occur below about 2.5 km from the surface.

The gas mass fraction X is calculated by assuming that the water vapor in the conduit is produced by the exsolution of water from magma and that no water inflow or outflow through the conduit wall takes place during the flow of magma from the magma chamber to the earth's surface. With this assumption the mass of water is conserved and we can write:

$$(M_G)_{\text{exsolved}} + (M_G)_{\text{dissolved}} = XM + Y(1-X)M = X_s M + Y_s(1-X_s)M = \text{constant} \quad (9)$$

or

$$X = \frac{X_s + Y_s(1-X_s) - Y}{1-Y} \quad (10)$$

where Y is the dissolved gas mass fraction in magma and Y_s and X_s pertain to the exsolution level z_s in the conduit (see Fig. 1). The dissolved gas mass fraction Y is computed on the basis of the composition and pressure of magma as discussed below in section 3.2. The use of Eqs. (5)–(8) in different two-phase flow regions of the conduit requires the specification of the appropriate constitutive equations for the interfacial drag between the phases F_{LG}, and for the frictional effects between the magma and conduit wall, F_{wL}, below the magma fragmentation region and the gas and conduit wall, F_{wG}, above the magma fragmentation region. These constitutive equations which are valid for the bubbly flow regime, where $0<\alpha\leqslant 0.75$, and for the gas-particle/droplet flow regime, where $0.75<\alpha<1$, are fully discussed by Dobran (1992) and are not reproduced here. We note, however, that the model also requires the use of an appropriate viscosity of magma which is dependent on the magma composition, and of an appropriate diameter of particles in the gas-particle/droplet flow regime above the magma fragmentation region. In the previous application of the model to the eruptions of Mt. St. Helens on May 18, 1980 and Vesuvius in A.D. 79 (Dobran, 1992), use was made of an empirical relation for the liquid magma viscosity which only accounts for the dissolved water content. In the present application of the model this deficiency is remedied and the compositional dependence of viscosity is taken into account.

The density of gas in the model can be accounted by an appropriate equation of state. For high temperatures appropriate to the flowing magma in the conduit, it is reasonable to employ for water vapor the perfect gas law $\rho_G = P/RT$, where R is the gas constant and T is the temperature. The validity of the ideal gas assumption was tested by a real gas equation of state (Harr et al., 1984) and found to produce negligible errors in the two-phase flow parameters in the conduit.

The above equations, together with the constitutive equations for F_{LG}, F_{wG}, F_{wL}, and composition-dependent density ρ_L and viscosity η_L of magma as discussed below, can be appropriately combined and numerically solved from $z=0$ to $z=L$ by specifying the conduit flow cross-sectional area A, conduit length L, conditions of magma in the magma chamber (temperature, pressure, and composition), stratigraphy of the volcano as discussed above, physical properties of magma and water vapor, and the mass flow-rate M (Dobran, 1992). In particular, these equations admit a maximum or critical flow-rate which for a constant diameter conduit produces the critical flow at the exit. For further details of the model, numerical solution procedure, and description of the computer program the reader is referred to Dobran (1992) and Dobran and Papale (1992).

3.2. *Gas exsolution modeling*

The modeling of gas exsolution from an ascending magma in a volcanic conduit can be performed by an approach which is similar to that of Nicholls (1980). In this model the water is assumed to be the only dissolved gas component and the exsolution is treated as an equilibrium process. With these assumptions, the chemical potentials of water vapor and dissolved water in magma must be identical, i.e.:

$$\mu^{G}_{H_2O}(P,T) = \mu^{L}_{H_2O}(x,P,T) \quad (11)$$

or after introducing the *standard state chemical potentials* $\mu^{oG}_{H_2O}(T)$ and $\mu^{oL}_{H_2O}(x,P,T)$, *fugacity* $f_{H_2O}(P,T)$, *partial molar volume* $\bar{V}_{H_2O}(x,P,T)$, and *activity* $a_{H_2O}(x,P,T)$, we have:

$$\mu^{oG}_{H_2O}(T)+RT\ln f_{H_2O}(P,T)=\mu^{oL}_{H_2O}(x,T)+\int_{P_{ref}}^{P}\bar{V}_{H_2O}(x,P,T)\mathrm{d}P+RT\ln a_{H_2O}(x,P,T) \quad (12)$$

where the superscript o refers to the standard state condition taken at atmospheric pressure ($P_{ref}=0.1$ MPa), x denotes the composition, and where the standard state chemical potential of water in the melt has been separated into contributions of pressure, and temperature and composition. Following Nicholls (1980), the standard state chemical potential of water vapor is given by:

$$\mu^{oG}_{H_2O}(T)=24.246T\ln T-8.0575\times10^{-3}T^2+5.7059\times10^{-7}T^3+647.92T^{1/2}-24.086\times10^4-18827T^{-1}-132.26T\ \mathrm{J/mol} \quad (13)$$

The molar volume of dissolved water can be obtained from a relation of Burnham and Davis (1974) which models the presence of water in albite. Thus:

$$\int_{P_{ref}}^{P}\bar{V}_{H_2O}(x,P,T)\mathrm{d}P=P[9.1485+3.6866\times10^{-3}T+1.1687\times10^{-5}T^2-1.9909\times10^{-9}T^3+P(6.1116\times10^{-3}-9.7283\times10^{-4}T-7.9032\times10^{-8}T^2)+P^2(1.5614\times10^{-2}+3.8147\times10^{-5}T)-9.9041\times10^{-4}P^3]\ \mathrm{J/mol} \quad (14)$$

where P is in MPa. The fugacity of water at temperature T and pressure P is obtained from the molar volume and reference state fugacity at temperature T and pressure $P=0.1$ MPa where the fugacity is close to one at high magmatic temperatures, i.e.:

$$\int_{P_{ref}}^{P}V_{H_2O}(P,T)\mathrm{d}P=RT[\ln f_{H_2O}(P,T)-\ln f_{H_2O}(P_{ref},T)] \quad (15)$$

with the molar volume V_{H_2O} being obtained from the steam tables (Harr et al., 1984). The activity of water in the liquid state can be found by extending to hydrous liquids the Gibbs free energy relation of magmas as given by Ghiorso et al. (1983). Thus:

$$a_{H_2O}(x,P,T)=x_{H_2O}\exp\left[\left(\sum_{i=1}^{n}w_{H_2O,i}x_i-\frac{1}{2}\sum_{i=1}^{n}\sum_{j=1}^{n}w_{ij}x_ix_j\right)\Big/RT\right] \quad (16)$$

where x_i denotes the molar fraction of component i in magma and n is the total number of components in the melt. The *symmetric binary interaction parameters* w_{ij} ($w_{ii}=w_{jj}$, $w_{ii}=0$) describe an attractive/repulsive behavior of each pair of molecules, and are independent of composition but not necessarily of pressure and temperature. Equation (16) contains an assumption that the molar volume and specific heat of mixing, V^{mix} and C_p^{mix}, are equal to zero as suggested by low-pressure experiments on magmas (Carmichael et al., 1977; Nelson and Carmichael, 1979). The consequences of these assumptions are that the Gibbs free energy of mixing G^{mix} is not anymore a function of P and that the excess Gibbs free energy G^{ex} is at most a linear function of T. A further assumption by Ghiorso et al. (1983) is that the anhydrous magma can be described by the *regular solution theory*[1] which gives that G^{ex} is independent of temperature. By extending this assumption to hydrous magmas it then follows

[1]For binary-type molecular interactions this assumption can be justified using the statistical mechanics theory, but for magmas it can be justified by the experimental data as originally suggested by Ghiorso and Carmichael (1980).

that the coefficients w_{ij} are independent of temperature and pressure at low pressures.

Equation (16) requires some further clarification. A number of works on the water solubility in silicate melts at both low pressures (Tomlinson, 1956; Russell, 1957) and high pressures (Hamilton et al., 1964; Hodges, 1974) suggested to many authors the following relation between the activity and mole fraction of water:

$$a_{H_2O} = k x_{H_2O}^2 \quad (17)$$

where k=constant for a low water content ($Y<0.06$ for andesitic melts, Hamilton et al., 1964). Burnham and Davis (1974) investigated the solubility of water in albite melts and found a relation similar to Eqn. (17) for $x_{H_2O}<0.5$, whereas for $x_{H_2O}\geq 0.5$ the activity of water was found to be an exponential function of the dissolved molar fraction of water. Nicholls (1980) applied the regular solution theory to hydrous silicate melts and found k to be a function of x_{H_2O} and anhydrous melt composition. This can also be accomplished on the basis of the equation from Ghiorso et al. (1983) for the Gibbs free energy of mixing of silicate melts, and extending their treatment to hydrous melts [Eqn. (16)]. However, both Nicholls (1980) and Ghiorso et al. (1983) used a relation in the form of Eqn. (17). The proportionality expressed by Eqn. (17) in albitic melts for $x_{H_2O}<0.5$ has been explained by Burnham and Davis (1974) on the basis of the reaction of H_2O with bridging oxygens and exchange of a proton and a Na cation. A similar, but more complex, mechanism involves an expulsion of Al^{3+} from a network-forming to a network-modifying position, as described by Mysen et al. (1980). In both cases the water is completely dissociated to form OH^- groups and no undissociated water is assumed to exist in the melt after hydration. In contrast, Stolper (1982a,b) and Silver et al. (1990) concluded from the infrared spectroscopic data that hydroxyl groups are the dominant hydrous species at low water contents (Y less than about 0.04), whereas the molecular water dominates at higher water contents. For rhyolitic glasses the mole fraction of molecular water was found to be proportional to the water fugacity for pressures less than 150 MPa (Silver et al., 1990). The existence of molecular water in hydrous silicate melts is also suggested by thermodynamics. Silver and Stolper (1985) described hydrous silicate melts as ideal mixtures of hydroxyl groups, H_2O molecules, and oxygens in the melt. This implies that for each species the activity coincides with the molar fraction and allowed Silver and Stolper to successfully reproduce the phase equilibria for the Ab-H_2O, Di-H_2O, and SiO_2-H_2O systems. Eggler and Burnham (1984) found that the thermodynamic relations described by Eqn. (17) do not apply to the system Di-H_2O. On the basis of the structural similarities between albite melts for $x_{H_2O}\geq 0.5$ and anhydrous diopside melts, both lacking a three-dimensional silicate network, they argued in favor of a relation between the activity and molar fraction of water similar to that found by Burnham and Davis (1974) for the system Ab-H_2O for $x_{H_2O}\geq 0.5$ at both low and high water contents. Finally, McMillan et al. (1986) and McMillan and Holloway (1987) discussed the proportionality between the fugacity and square of the water molar fraction as expressed by Eqn. (17). Based on a consideration that high-pressure solubility measurements were carried out by many researchers as a function of varying total pressure and hence give polybaric points on the water saturation surface, they argued that the observed relations as described by Eqn. (17) are entirely fortuitous. In addition, McMillan and Holloway (1987) revised a number of water solubility determinations and found that the bulk of data do not follow such a relation. In conclusion, there is no good reason to assume that Eqn. (17) describes the relation between activity and mole fraction of dissolved water, and we assumed instead the following relation:

$$a_{H_2O} = k x_{H_2O} \quad (18)$$

TABLE 2

Source data for the standard state chemical potential of water

Composition	P (MPa)	T (K)	x_{H_2O}	Ref.
C.R. Basalt	103.4	1373	0.1043	1
C.R. Basalt	200	1372	0.1495	1
Mt.Hd. Andesite	103.4	1373	0.1457	1
Mt.Hd. Andesite	200	1373	0.1891	1
Albite	100	1203	0.1182	2
Albite	100	1193	0.1214	2
Albite	100	1193	0.1296	2
Albite	50	1238	0.0857	2
Albite	50	1238	0.0699	2
Albite	200	1123	0.1864	2
$Ab_{70}Or_{30}$	50	1203	0.0756	2
$Ab_{70}Or_{30}$	50	1203	0.0757	2
$Ab_{70}Or_{30}$	100	1123	0.1353	2
$Ab_{70}Or_{30}$	200	1083	0.1940	2
$Ab_{70}Or_{30}$	100	1143	0.1477	2
$Or_{56}Q_{44}$	50	1123	0.0828	2
$Or_{56}Q_{44}$	100	1098	0.1163	2
$Or_{56}Q_{44}$	200	1043	0.1706	2
$Or_{56}Q_{44}$	50	1123	0.0683	2
$Ab_{64.5}Q_{35.5}$	100	1123	0.1359	2
$Ab_{64.5}Q_{35.5}$	200	1043	0.1988	2
$Ab_{55.2}Q_{44.8}$	50	1163	0.0670	2
$Ab_{36.8}Or_{26.4}Q_{36.8}$	200	973	0.1791	2
$Ab_{36.8}Or_{26.4}Q_{36.8}$	200	973	0.2000	2
$Ab_{36.8}Or_{26.4}Q_{36.8}$	300	963	0.2794	2
$Ab_{36.8}Or_{26.4}Q_{36.8}$	100	1003	0.1297	2
$Ab_{36.8}Or_{26.4}Q_{36.8}$	50	1063	0.0950	2
$Ab_{36.8}Or_{26.4}Q_{36.8}$	100	1003	0.1434	2
$Ab_{36.8}Or_{26.4}Q_{36.8}$	50	1013	0.0950	2
$Ab_{47}Or_{23}Q_{30}$	400	933	0.2622	2
$Ab_{47}Or_{23}Q_{30}$	400	933	0.2730	2
Albite	200	1143	0.2006	3
Albite	500	1053	0.2856	3
Albite	490	1053	0.2810	3
Harding Pegmatite	207	943	0.1995	3
Harding Pegmatite	410	963	0.2966	3
Harding Pegmatite	740	963	0.3791	3
Harding Pegmatite	590	963	0.3313	3

[1]Hamilton et al. (1964).
[2]Tuttle and Bowen (1958).
[3]Burnham and Jahns (1962).

which is implicit in Eqn. (16), with k obtained from the regular solution theory which holds for an exponential dependence of a_{H_2O} on x_{H_2O} (see also Eqn. (20) below). Equation (18) is preferred, since we found that it fits better the experimental data (Tuttle and Bowen, 1958; Hamilton et al., 1964; Burnham and Jahns, 1962; Kogarko et al., 1977) than Eqn. (17).

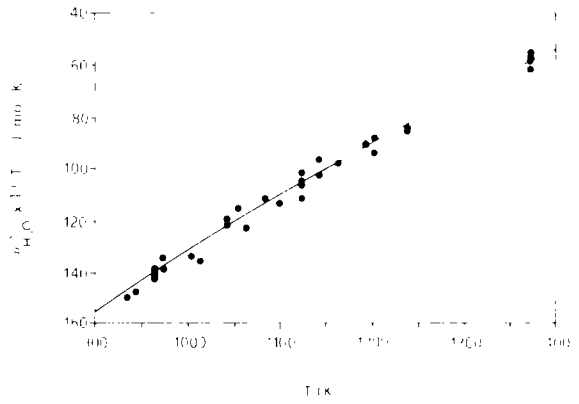

Fig. 3. Distribution of the pressure independent standard state chemical potential of water in magmas with temperature for the compositions reported in Table 2. In spite of a large compositional spectrum all data can be represented well by a single curve.

In determining the standard-state chemical potential of water in magma, we adopted the w_{ij} coefficients given by Ghiorso et al. (1983) and hence referred to a system of complex oxides (Ghiorso et al., 1983, table 4) instead of the normal oxides to which chemical compositions are usually referred to. Employing a large number of experimentally determined water solubilities of different magmatic liquids as shown in Table 2, it was found that in spite of the large number of assumptions as discussed above and the large compositional spectrum, all data fit very well with temperature as illustrated in Figure 3. The fit of data points in this figure can be expressed by the following equation:

$$\mu^{oL}_{H_2O}(x,T) = -428.79T + 36.507 \times 10^{-2}T^2 - 6.9419 \times 10^{-5}T^3 \text{ J/mol} \quad (19)$$

A similar functional relationship was also found by Nicholls (1980) who employed the compositional dependence of activity of water as a parameter of the regression curve, instead of independently computing it. The exsolution curves for the white and gray pumice compositions are illustrated in Figure 4. These curves

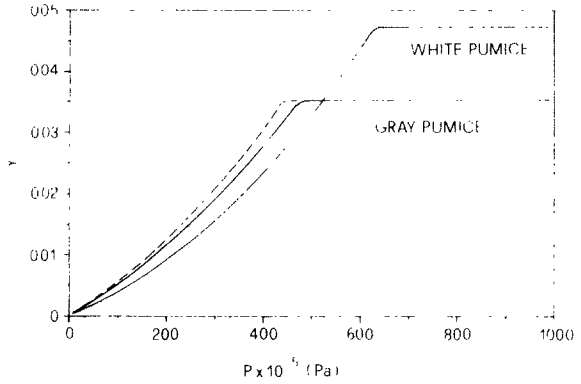

Fig. 4. Exsolution curves for the white and gray magma compositions of the A.D. 79 eruption of Vesuvius. They were obtained by considering an initial water mass fraction and temperature of 0.047 and 1073 K for the white, and 0.035 and 1123 K for the gray magma. The dashed curve represents the gray magma with a temperature of 1073 K.

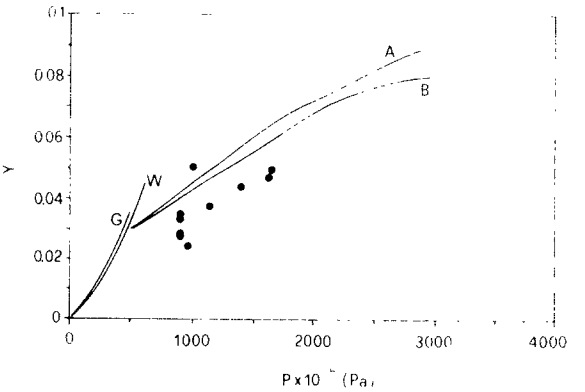

Fig. 5. Comparison between the low-pressure white (W) and gray (G) magma exsolution curves determined by the model described in the text, and the experimentally determined high-pressure water contents for liquids of alkaline compositions. A = eudialyte pegmatite; B = melanocratic foyaite, after Kogarko et al. (1977). The dark points correspond to the artificial silicate system SiO_2-Al_2O_3-Na_2O-K_2O, after Dingwell et al. (1984).

correspond to the maximum water content of 4.7 wt.% for the white pumice magma and 3.5 wt.% for the gray pumice magma, as obtained by the "difference" method using melt inclusion analyses (Sigurdsson et al., 1990). In the determination of the exsolution curves of white and gray magmas, two different temperatures of 1073 and 1123 K were adopted. This was suggested by the mineralogical assemblage and the composition of mechanically separated glasses of pumice samples of the two different magmas (Barberi et al., 1981). The exsolution curve of the gray magma for $T=1073$ K is also illustrated in Figure 4 as a dashed curve and shows that a deviation of several tens of degrees does not modify significantly the results. From these results it is seen that the white magma begins to exsolve at $P=62.6$ MPa, whereas the gray magma begins to exsolve at $P=47.6$ MPa.

High-pressure solubility curves for liquids of alkaline compositions as experimentally determined by Kogarko et al. (1977) and Dingwell et al. (1984) show solubilities which are greater than those typical of granitic melts. These high-pressure solubility curves are shown in Figure 5 and appear to merge well with our low pressure curves. The exsolution characteristics of different magmas determine the exsolution length z_s and fragmentation length z_f in a conduit when used in the above nonequilibrium model.

By referring to Figure 4 it is seen that while the gray magma has a higher solubility than the white magma, its water content is lower. This is perhaps not obvious and requires a closer investigation of the consistency between the solubility model, experimental data, and molecular solubility mechanism.

For the purpose of verifying the consistency of the compositional effects on water solubility of both gray and white magmas as predicted by the model, Figure 6 illustrates the contribution to the activity of water by each component. This figure illustrates the anhydrous compositional dependence of activity of water ϑ as a function of composition which can be found by rewriting Eqn. (16) in the following form:

$$a_{H_2O}(x,T,P)=x_{H_2O}\exp\left(\frac{\vartheta(1-x_{H_2O})^2}{T}\right) \tag{20}$$

An increasing concentration of a component

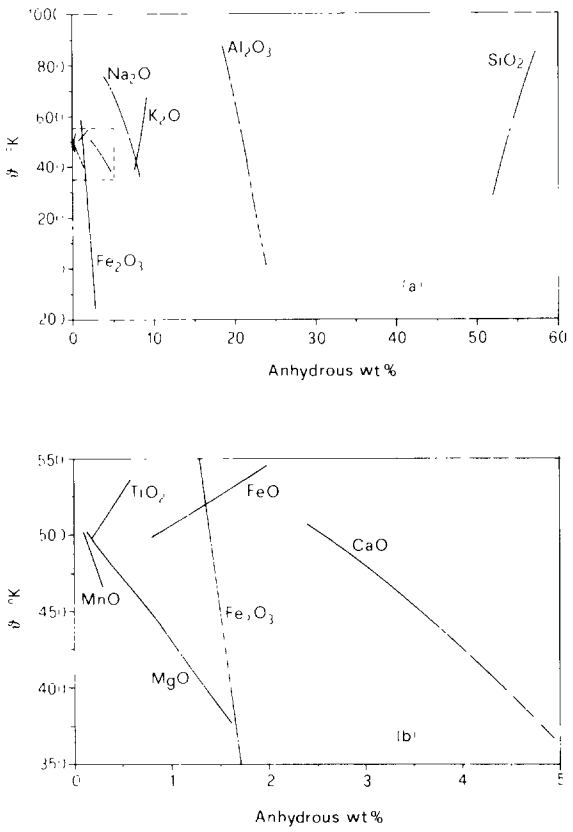

Fig. 6. (a) The anhydrous compositional dependence of activity of water (ϑ) plotted against the concentration of each component for the range of compositions from the white to the gray magmas. See text for detailed explanation. (b) Enlargement of the dashed region in (a).

produces a decrease in the water solubility if it is positively correlated with ϑ, and an increase in the water solubility if it is negatively correlated with it. It should be stressed, however, that although the results in Figure 6 reflect the general contribution of each component they are strictly valid only to the above referred magma compositions. For example, the interaction between SiO_2 and H_2O is characterized by a slightly negative value of relative interaction coefficient w_{ij} (Table A4-3 in Ghiorso et al., 1983), which reflects a slightly attractive behavior. Nevertheless, an increase in the SiO_2 concentration in the A.D. 79 magma results in a decrease of water solubility, since it involves a parallel decrease in the concentrations of all other components with a net effect which is not simply predictable. A similar effect is shown by the interaction between K_2O and H_2O which is also characterized by a negative w_{ij} coefficient, whereas an increase in the K_2O content in the A.D. 79 magma produces a decrease in water solubility (Fig. 6). As Figure 6 illustrates, an increase of Na_2O and Al_2O_3 greatly increases the solubility of water. This is consistent with Mysen et al. (1980) and Mysen (1988) who found, on the basis of spectroscopic analyses of hydrous magmas, that the water in aluminosilicates enters in the form of OH-complexes bonded to both Al^{3+} (octahedral) and Na^+ as well as molecular H_2O, but not as Si-OH. The infrared spectroscopic analyses performed by Stolper (1982b) suggest, however, a less abundance of the Na-OH complex and indicate that hydroxyl groups are bound principally to Si and/or Al cations, without being able to descriminate between them. Remmele et al. (1986) obtained Raman spectra of hydrous aluminosilicate melts and suggested the presence of Al-OH and absence of Si-OH complexes. The presence of Ca-OH complexes is reported by Mysen and Virgo (1986), which is also consistent with the predictions of the model as shown in Figure 6. Furthermore, Fe_2O_3 is found to have a great affinity with water (see Fig. 6) as may be justified on the basis of the structural and chemical analogies between Fe^{3+} and Al^{3+}, which is demonstrated to play an important role in the water solubility mechanism (Epel'baum, 1985; Oxtoby and Hamilton, 1978; Manning et al., 1980; Mysen et al., 1980; Stolper, 1982b; Remmele et al., 1986). Finally, the effect of MgO in Figure 6b is to increase the water solubility, whereas in the considered compositional range MnO, TiO_2 and FeO have only a minor effect. The trends in Figure 6 are also consistent with data from McMillan and Holloway (1987). By revising many experimental water solubility determinations, they found an increase in water solubility with decreasing SiO_2 and increasing Na_2O, Al_2O_3, CaO, and K_2O contents in simple binary systems, and a

greater effect in increasing solubility associated to alkali systems as compared to alkaline-earth systems. However, McMillan and Holloway found a lower effect of Al_2O_3 on water solubility than suggested in Figure 6. From this discussion it follows that the higher solubility of the gray than of the white magma is brought about by its higher CaO, Fe_2O_3, MgO and lower SiO_2 contents, whose effects counteract and exceed those of lower Na_2O and Al_2O_3 contents.

A possible explanation of less abundance of water in the gray than in the white magma, in spite of its higher solubility at a given pressure, is in its higher content of biotite (the only hydrated crystal present in the A.D. 79 magma, with the exception of a rare amount of amphibole), whose crystallization determines a depletion in the water content of the melt. Starting from the data on the distribution of crystals in pumice samples of the white and gray compositions (Civetta et al., 1991) and on pumice and liquid densities, we estimated the mean concentration of biotite in both white and gray magmas prior to the eruption (see section 3.4). Unfortunately, the available data on the composition of biotite of the A.D. 79 eruption are usually presented without accounting for the water content. Chemical analyses of biotites from many different worldwide igneous rocks show, however, a structural water content from 1 to 4 wt.% (Deer et al., 1962). By using these values and starting from an initial water content of 5 wt.%, the crystallization of an amount of biotite corresponding to that of the white magma produces a maximum depletion to a final water content from 4.85 to 4.99 wt.%, whereas the crystallization of an amount corresponding to that of the gray magma produces a maximum depletion to final values from 4.55 to 4.94 wt.%. It follows that the presence of the biotite crystals in the magma is not sufficient to explain the observed distribution of water between the white and gray magmas, and that alternative effects should be responsible for this large difference.

A migration of water within a magma chamber can result from a gradient in its chemical potential. This in turn can be produced by a compositional, pressure, or temperature gradient (see Eqn. 12). In discussing the equilibrium condition in different regions of a magma chamber, an account must also be taken of the gravitational potential field in which the magma is immersed. Under this condition, the chemical equilibrium for water is given by the constancy of the sum of chemical and gravitational potentials (Modell and Reid, 1974), i.e.:

$$\mu_{H_2O} + m_{H_2O} g z = \text{constant} \tag{21}$$

where m_{H_2O} is the molecular weight of water. By substituting the water chemical potential from Eqn. (12) into the above equation, we obtain:

$$\int_{P_{ref}}^{P_1} \bar{V}_{H_2O}(x_1, T_1)\,dP - \int_{P_{ref}}^{P_2} \bar{V}_{H_2O}(x_2, T_2)\,dP + \mu^{0L}_{H_2O}(x_1, T_1) - \mu^{0L}_{H_2O}(x_2, T_2) - m_{H_2O} g (z_2 - z_1) = RT_2 \ln a_{H_2O}(x_2, T_2) - RT_1 \ln a_{H_2O}(x_1, T_1) \tag{22}$$

where the subscripts 1 and 2 refer to the two different points in the magma chamber, and where the pressures in the magma chamber are related by the following hydrostatic relation:

$$P_1 = P_2 + \int_{z_1}^{z_2} \rho_L g \, dz \tag{23}$$

where ρ_L is the local magma density in the magma chamber. Equation (22) can now be used to infer the equilibrium water distribution in the magma chamber prior to the eruption of Vesuvius in A.D. 79, with the result that in spite of the greater solubility of water in the gray magma, the pressure gradient in the chamber is able to stabilize a higher water content in the top white magma than in the gray magma on the bottom. Without a temperature gradient in the chamber and taking the white

magma water content of 4.7 wt.% and gray magma water content of 3.5 wt.%, the required pressure difference in the chamber is 190 MPa, which is clearly an unreasonable value since it corresponds to a minimum magma chamber depth of more than 8 km. As shown in Figure 7a, this large value is greatly reduced if a downward temperature gradient is introduced. A difference in temperature between the bottom and the top of the magma chamber of only 20 K reduces the required pressure difference to about 9.4 MPa — a value which gives a minimum magma chamber depth of about 400 m, which is consistent with both an estimated volume of erupted magma of about 3.6 km^3 (Carey and Sigurdsson, 1987) and an estimated diameter of the magma reservoir of about 3 km (Sigurdsson et al., 1990). If, instead, a compositionally homogeneous magma with a composition similar to that of the gray magma is considered, the effect of a given temperature difference is increased. In addition, a change in the absolute temperature of the system up to about 150 K does not produce a significant difference in results (Fig. 7a).

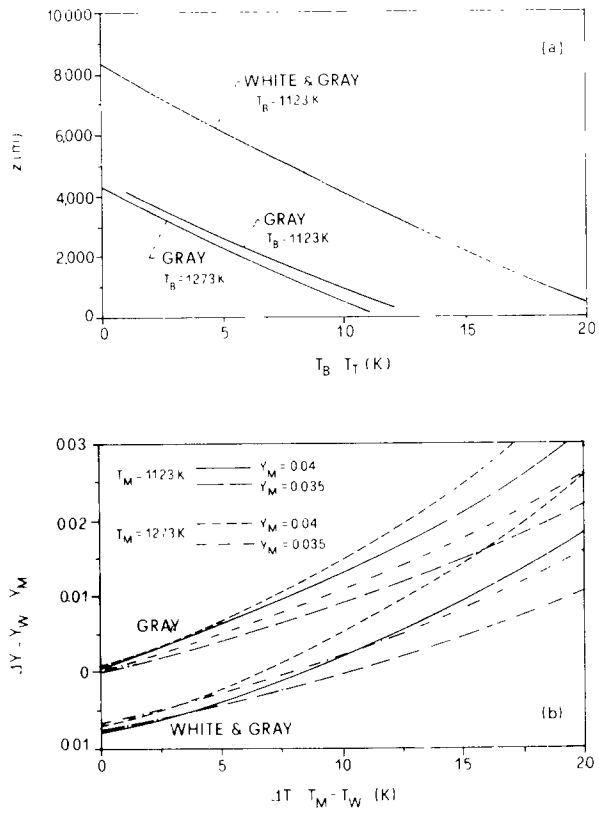

Fig. 7. (a) Distribution of the minimum magma chamber height consistent with the observed water contents with the difference between the bottom (T_B) and top (T_T) temperatures and for the magma chamber of the A.D. 79 eruption of Vesuvius. (b) Distribution of the dissolved water content with the temperature difference between the magma chamber interior and near-wall magma in the absence of the pressure gradient. See text for further explanation.

The temperature differences in a magma chamber can be produced by several mechanisms, such as by mixing of a hot magma with a pre-existing cooler and more differentiated magma, heat transfer between magma and the surrounding walls of the chamber, and by melting and assimilation of the wall and roof rocks. A temperature difference between the bulk magma in the chamber and the surrounding wall rocks can produce a chemical potential gradient which can also trigger water migration. This can be established from Eqn. (22) by setting $z_1 = z_2$ and $P_1 = P_2$. Figure 7b illustrates the difference ΔY between the equilibrium water contents of magma near a cold wall and at the bulk interior as a function of the temperature difference ΔT between these two regions, for two different bulk magma temperatures, water contents and magma wall compositions, and for the gray magma composition at the magma chamber interior. When considering a white magma at the chamber walls, an inward (from the wall towards the magma chamber interior) migration of water occurs for ΔT of less than about 10 K, and no gradient of dissolved water content occurs for ΔT between about 6 and 12 K, with the exact values depending on the magma chamber interior water content and temperature. For a homogeneous magma composition in the chamber, a similar ΔT produces an equilibrium difference in the dissolved water content between near-wall and interior magmas which is close to that found between the A.D. 79 white

and gray magmas ($\Delta Y \approx 0.01$). In both cases an increase in the magma chamber temperature or in its water content produces and increased water transfer from the magma chamber interior to the wall region.

The above discussions assume that magmas in magma chambers do not convect or crystallize. In reality this is not the case. The temperature differences in the chamber also produce convection, crystallization, and liquid fractionation whereby a more evolved, water-enriched, and less dense magma is generated and accumulated near the roof of the magma chamber (Shaw, 1965, 1974; Spera et al., 1984; Lowell, 1985; McBirney et al., 1985; Nilson et al., 1985; Trial and Spera, 1988, 1990). These magma chamber processes are considered to be much more important in determining the compositional variation of magma than the equilibrium processes discussed above, and should, therefore, produce a more effective migration of water towards the magma chamber roof. Nevertheless, the equilibrium results in Figure 7b provide a trend for the water migration which is consistent with a larger proportion of dissolved water in the white magma, and provide a reasonable estimate of the water migration trend during the initial stages of the A.D. 79 magma chamber existence when magma differentiation processes were not yet established and magma temperatures were higher.

To summarize, the distribution of water between the white and gray magmas prior to the eruption of Vesuvius in A.D. 79 does not appear to be only a function of the water solubility of magmas, but also depends on the existence of temperature and pressure gradients in the chamber. The existence of even a small temperature gradient is consistent with the observed water contents of the white and gray magmas.

3.3. Magma viscosity modeling

The viscosity of a magmatic liquid depends on various factors, including temperature, composition, pressure, and crystallinity (McBirney and Murase, 1984). The temperature has a significant effect in reducing the magma viscosity; this has been well demonstrated for basaltic magmas at low pressures (Murase and McBirney, 1973; Scarfe, 1981) and at high pressures (Kushiro, 1986). The water in magmas is also very important, since it produces a depolymerization of the silicate network and lowering of the magma viscosity (Mysen, 1988).

In the modeling of magma viscosity use was made of the Arrhenius mixture rule (Bondi, 1967; Shaw, 1972):

$$\ln\eta = \sum_{i=1}^{n} x_i \ln\eta_i \qquad (24)$$

where η is the viscosity of the multicomponent mixture and η_i is some characteristic viscosity contribution of component i with mole fraction x_i. For the silicate liquids, the contribution of each component in the mixture can be determined by averaging the behavior of synthetic systems of relatively few constituents (Bottinga and Weill, 1972). Using this approach, Shaw (1972) developed a simple method to estimate magma viscosities as a function of composition and temperature at atmospheric pressure. In this method the water is simply treated as one of the components of the mixture, so that its contribution to the viscosity can be estimated as for other oxides. The independence of viscosity on pressure, which is assumed in the method of Shaw, is justified by the experimental data on basaltic liquids and simple silicate systems to within several hundreds megapascals (Kushiro, 1976, 1978, 1981, 1986). Based on this viscosity model, the crystal-free viscosity curves for the white and gray magma compositions are shown in Figure 8 as a function of the water content.

A major difficulty arises, however, when considering the effects of crystals on magma viscosity. The various approaches which have been used in the past for this purpose involve

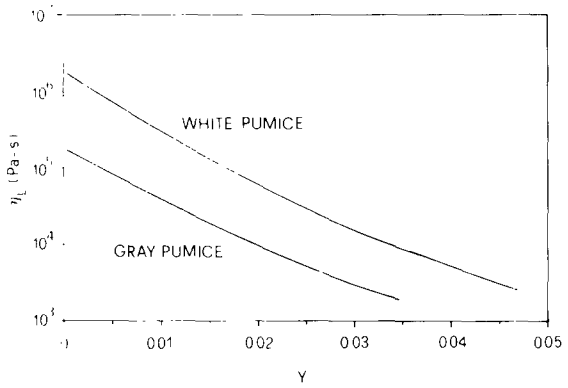

Fig. 8. Crystal-free magma viscosity distribution with the dissolved water mass fraction for the white and gray magmas.

two different relations which produce dramatically different results. As a consequence, the physics of magma flow in the conduit of Vesuvius will be employed to establish the possible constraints on different crystal viscosity models. These are:

The Einstein–Roscoe Equation

$$\frac{\eta_L}{\eta_L^\circ} = (1 - \bar{R}\phi_L)^{-2.5} \tag{25}$$

where η_L/η_L° is the ratio of the liquid magma viscosity with crystals to that without crystals, ϕ_L is the crystal volume fraction in the liquid, and $\bar{R}$ is a factor based on the volumetric fraction of solids at their maximum packing which for spheres of uniform size is 1.35 and for serial texture is equal to unity. Marsh (1981) found, however, that a value of this parameter equal to 1.67 fits well with the measured viscosities of the Aleutian lavas. In addition, a modification of the above equation has been successfully employed in the two-phase flow applications to nonsilicate systems (Ishii and Zuber, 1979), and more recently to magma flow in conduits (Dobran, 1992), i.e.:

$$\frac{\eta_L}{\eta_L^\circ} = \left(1 - \frac{\phi_L}{1-\phi_L}\right)^{-2.5(1-\phi_L)} \tag{26}$$

Modified Sherman Equation

McBirney and Murase (1984) and Murase et al. (1985) proposed the following modification of the Sherman's equation (Sherman, 1968) for crystal-bearing magmas:

$$\frac{\eta_L}{\eta_L^\circ} = \exp\left[\frac{0.019 d_C}{\phi_L^{-1/3} - 1}\right] \tag{27}$$

where d_C is the mean crystal diameter expressed in microns, and found that the experimental data on the Mt. St. Helens dacitic dome can be well correlated with this equation.

The Einstein–Roscoe and modified Sherman's relations are illustrated in Figure 9 for the crystal diameters of 200 and 500 μm. This range probably embraces the mean crystal diameter for both the white and gray magmas of the A.D. 79 eruption, as can be inferred from Barberi et al. (1989) who showed that the crystal diameter of both magma phases typically range from 60 μm to 4 mm. It may be noted from this figure that the relation of Sherman (Fig. 9b) predicts a much larger varia-

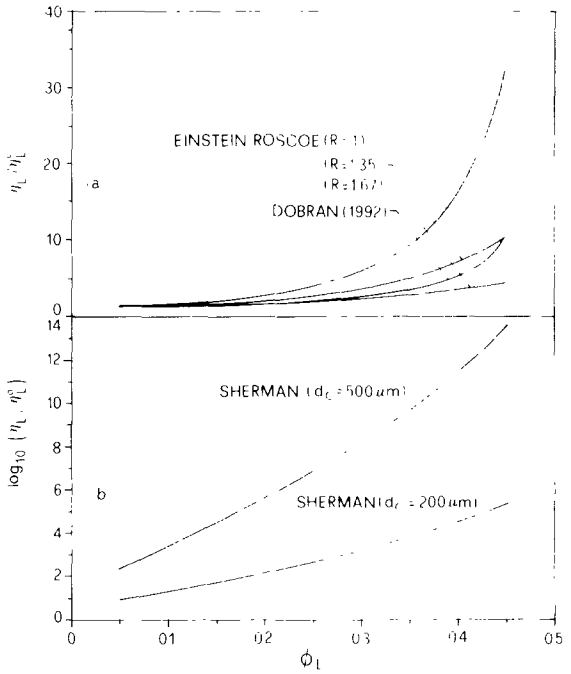

Fig. 9. Crystal viscosity ratio η_L/η_L° distribution with crystal volume fraction for: (a) Einstein–Roscoe relations and relation after Dobran (1992); (b) Sherman's relation with mean crystal diameters of 200 and 500 μm.

tion of viscosity, for a constant crystal volume fraction, than that of Einstein–Roscoe (Fig. 9a). It may be noted that the viscosity of a suspension of solid spheres at a given concentration depends on the size distribution, but not on the absolute size of particles (Clayton, 1954), as in Sherman's formula. In this paper some constraints will be given to the applicability of the above crystal viscosity relations during the eruption of Vesuvius in A.D. 79 and their consistency with the physical model of magma flow in the conduit.

3.4. Magma density

The densities of white and gray magmas were computed using the model equation of silicate liquid volumes of Lange and Carmichael (1987) which was obtained from experimental data of the partial molar volumes of oxides:

$$\rho_{Lo} = \frac{\sum_{i=1}^{n-1} (x_i m_i + x_{H_2O} m_{H_2O})}{\sum_{i=1}^{n-1} (x_i \bar{V}_i + x_{H_2O} \bar{V}_{H_2O} + x_{Na_2O} x_{TiO_2} \bar{V}_{Na_2O-TiO_2})} \quad (28)$$

This model accounts for the effects of oxidation state and pressure, but in our use of this model it was found that these effects are minor in the pressure range from 0.1 to 100 MPa or for pressures typical in the conduit of Vesuvius during the eruption in A.D. 79.

The liquid densities obtained above require an adjustment for the presence of crystals in magma according to the following expression:

$$\rho_L = (1-\phi_L)\rho_{L0} + \sum_{i=1}^{n} \phi_{Li}\rho_{Li} \quad (29)$$

where ρ_L is the density of liquid magma which includes crystals, ϕ_L is the total crystal volume fraction in the liquid, ρ_{Lo} is the crystal-free liquid density (2200 kg/m^3 for the white and 2325 kg/m^3 for the gray magma, as determined in this work), and ϕ_{Li} is the crystal volume fraction and ρ_{Li} the density of the ith crystal in the liquid.

The modal estimates of the phenocrysts content in the white and gray pumice are given by Civetta et al. (1991). These estimates show a greater abundance of minerals in the gray pumice which can be related to a higher phenocryst content of the gray magma with respect to the white one which has been explained in terms of a gravity-induced differentiation process within the magma chamber (Barberi et al., 1981). The volume fraction of crystals in the liquid prior to the eruption should be evaluated, however, by taking into account the different vesiculation of white and gray pumice. The vesiculation, crystallinity, and mass fraction of each component in the magma prior to the eruption can be obtained from the following equations:

$$Ve = 1 - \frac{\rho_P(1-Ve)}{\rho_{Lo}(1-Ve) + \sum_{i=1}^{n} \phi_{Pi}(\rho_{Li} - \rho_{Lo})} \quad (30)$$

$$\phi_{Li} = \frac{\phi_{Pi}}{(1-Ve)}, \quad \sum_{i=1}^{n} \phi_{Li} = \phi_L = \frac{\phi_P}{1-Ve} \quad (31)$$

$$W_{Li} = \frac{\rho_{Li}\phi_{Li}}{\sum_{i=1}^{n} \rho_{Li}\phi_{Li} + \rho_{Lo}(1-\phi_L)}, \quad \sum_{i=1}^{n} W_{Li} = W_L \quad (32)$$

where Ve is the vesiculation, ρ_P is the bulk density of the pumice (620 kg/m^3 for the white and 1000 kg/m^3 for the gray pumice, and both referred to the < -4 phi class, Barberi et al., 1989), ϕ_{Pi} is the modal pumice content of the ith crystal, W_{Li} is the crystal mass fraction of the ith crystal in the liquid prior to the eruption, ϕ_L is the total crystal volume fraction and W_L is the total crystal mass fraction in the liquid, and ϕ_P is the total crystal volume fraction in the pumice. In Eqns. (31) it is assumed that the crystals in the samples of white and gray pumice are the same as in the corresponding magmas. The results, which are given in Table

TABLE 3

Vesiculation and liquid porfiricity of white and gray pumice

Pumice/magma type		White	Gray
Ve		0.744 ± 0.008	0.600 ± 0.010
ϕ_L		0.241 ± 0.090	0.234 ± 0.068
W_L		0.296 ± 0.123	0.291 ± 0.093
	ϕ_{P_1}	0.031 ± 0.007	0.008 ± 0.003
K-feldspar	ϕ_{L_1}	0.122 ± 0.031	0.020 ± 0.008
	W_{L_1}	0.132 ± 0.037	0.021 ± 0.009
	ϕ_{P_1}	0.021 ± 0.006	0.048 ± 0.009
Clinopyroxene	ϕ_{L_1}	0.083 ± 0.026	0.121 ± 0.026
	W_{L_1}	0.108 ± 0.035	0.150 ± 0.033
	ϕ_{P_1}	0.004 ± 0.003	0.029 ± 0.007
Biotite	ϕ_{L_1}	0.016 ± 0.012	0.073 ± 0.019
	W_{L_1}	0.021 ± 0.016	0.088 ± 0.024
	ϕ_{P_1}	0.002 ± 0.002	0.004 ± 0.002
Leucite	ϕ_{L_2}	0.008 ± 0.008	0.010 ± 0.005
	W_{L_1}	0.010 ± 0.010	0.010 ± 0.005
	ϕ_{P_1}	0.002 ± 0.002	0.003 ± 0.003
Fe-Ti oxides	ϕ_{L_2}	0.008 ± 0.008	0.008 ± 0.008
	W_{L_1}	0.018 ± 0.018	0.018 ± 0.018
	ϕ_{P_1}	0.001 ± 0.001	0.001 ± 0.001
Garnet	ϕ_{L_1}	0.004 ± 0.004	0.003 ± 0.003
	W_{L_1}	0.007 ± 0.007	0.004 ± 0.004

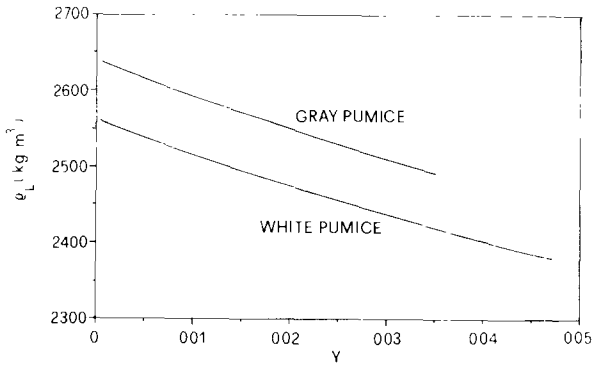

Fig. 10. Magma density (including crystals) dependence on the dissolved water mass fraction for the white and gray magmas.

3, show comparable values of the white and gray liquid crystal contents, even if significant differences in the concentration of each crystal species do exist. The resulting magma densities are shown in Figure 10 as a function of water content. The difference between the gray and white magma densities ranges from 111 kg/m^3 in the magma chamber to 78 kg/m^3 for anhydrous magma conditions. These densities are, moreover, very similar to those reported by Sigurdsson et al. (1990).

3.5. Input data for the simulations

The utilization of the two-phase flow model as described in section 3.1 for the simulation of magma flow in the conduit during the A.D. 79 eruption of Vesuvius requires the specification of conditions in the magma chamber, conduit geometry, and of the stratigraphy of the conduit wall rocks. Although this model assumes steady-state conditions of magma in the conduit, it may be noted that non-steady phenomena such as conduit wall erosion, wall collapse, and variations in the mass discharge rate up to one order of magnitude may had occurred (Wilson et al., 1980). When long duration of the plinian eruption phase is compared with the significant variations of the deposit (Lirer et al., 1973; Sigurdsson et al., 1982, 1985; Carey and Sigurdsson, 1987; Santacroce, 1987) it is permissible to consider, however, the eruption as quasi steady-state which allows the utilization of the above conduit flow model. During this quasi steady-state process it is then possible to model the maximum discharge rates of the white (8×10^7 kg/s) and gray (1.5×10^8 kg/s) magmas by assuming that these flow-rates are the maximum possible discharges through the conduit, which corresponds to the choked-flow condition at the conduit exit. In reality, the presence of a crater (which is not included in modeling) at the exit of a conduit enables the flow to become supersonic at the exit of the crater, but it will remain sonic at the exit of the conduit. In the following discussion the references to the conduit exit pertain, therefore, to the base of the crater where the flow exits from a conduit.

The depth of the magma chamber of Vesu-

TABLE 4

Input data for the simulations

White magma: $M=8\times10^7$ kg/s, choked flow, $\rho_L=2400$ kg/m^3, $T_o=1073$ K, $Y_o=0.047$

$L=3$ km ($P_o=74.7$ MPa)		$L=5$ km ($P_o=124.7$ MPa)	
$d_p=2$ cm $D=80$–120 m	$d_p=200$ μm $D=80$–120 m	$d_p=2$ cm $D=70$–120 m	$d_p=200$ μm $D=80$–120 m

Gray magma: $M=1.5\times10^8$ kg/s, choked flow, $\rho_L=2550$ kg/m^3, $T_o=1123$ K, $Y_o=0.035$

$L=3$ km ($P_o=74.7$ MPa)		$L=5$ km ($P_o=124.7$ MPa)	
$d_p=2$ cm $D=80$–140 m	$d_p=200$ μm $D=80$–140 m	$d_p=2$ cm $D=80$–140 m	$d_p=200$ μm $D=80$–140 m

White magma: $\eta_L/\eta_L^0=1$, choked flow, $\rho_L=2400$ kg/m^3, $T_o=1073$ K, $Y_o=0.047$

$L=3$ km ($P_o=74.7$ MPa)		$L=5$ km ($P_o=124.7$ MPa)	
$d_p=2$ cm $M=7.2\times10^7$–8.8×10^7 kg/s	$d_p=200$ μm $M=7.2\times10^7$–8.8×10^7 kg/s	$d_p=2$ cm $M=7.2\times10^7$–8.8×10^7 kg/s	$d_p=200$ μm $M=7.2\times10^7$–8.8×10^7 kg/s

Gray magma: $\eta_L/\eta_L^0=1$, choked flow, $\rho_L=2550$ kg/m^3, $T_o=1123$ K, $Y_o=0.035$

$L=3$ km ($P_o=74.7$ MPa)		$L=5$ km ($P_o=124.7$ MPa)	
$d_p=2$ cm $M=1.35\times10^8$–1.65×10^8 kg/s	$d_p=200$ μm $M=1.35\times10^8$–1.65×10^8 kg/s	$d_p=2$ cm $M=1.35\times10^8$–1.65×10^8 kg/s	$d_p=200$ μm $M=1.35\times10^8$–1.65×10^8 kg/s

White magma: $D=140$ m, non-choked flow, $\rho_L=2400$ kg/m^3, $T_o=1073$ K, $Y_o=0.047$

$L=3$ km ($P_o=74.7$ MPa)		$L=5$ km ($P_o=124.7$ MPa)	
$d_p=2$ cm $M=6.8\times10^7$–9.2×10^7 kg/s	$d_p=200$ μm $M=6.8\times10^7$–9.2×10^7 kg/s	$d_p=2$ cm $M=6.8\times10^7$–9.2×10^7 kg/s	$d_p=200$ μm $M=6.8\times10^7$–9.2×10^7 kg/s

Gray magma: $D=200$ m, non-choked flow, $\rho_L=2550$ kg/m^3, $T_o=1123$ K, $Y_o=0.035$

$L=3$ km ($P_o=74.7$ MPa)		$L=5$ km ($P_o=124.7$ MPa)	
$d_p=2$ cm $M=1.3\times10^8$–1.7×10^8 kg/s	$d_p=200$ μm $M=1.3\times10^8$–1.7×10^8 kg/s	$d_p=2$ cm $M=1.3\times10^8$–1.7×10^8 kg/s	$d_p=200$ μm $M=1.3\times10^8$–1.7×10^8 kg/s

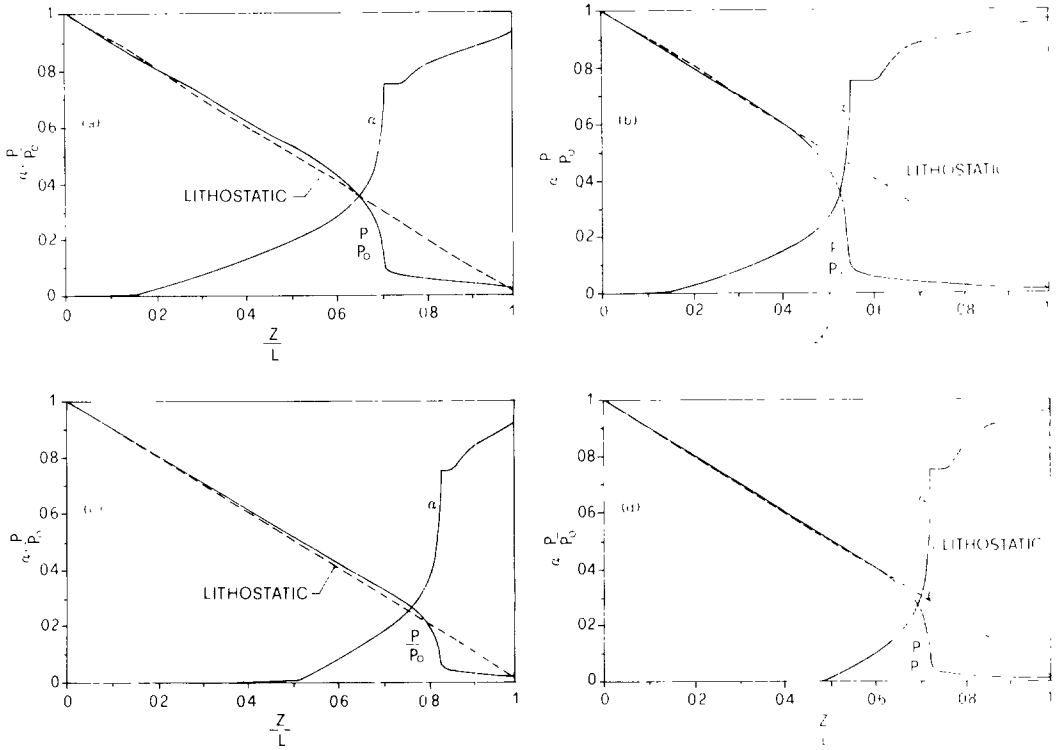

Fig. 11. Pressure and gas volumetric fraction variations along the conduit for the white magma and particle size of 200 μm. The dashed line corresponds to the lithostatic pressure distribution by accounting for the stratigraphy of conduit. (a) $L=3$ km, $D=80$ m; (b) $L=3$ km, $D=120$ m; (c) $L=5$ km, $D=80$ m; (d) $L=5$ km, $D=120$ m.

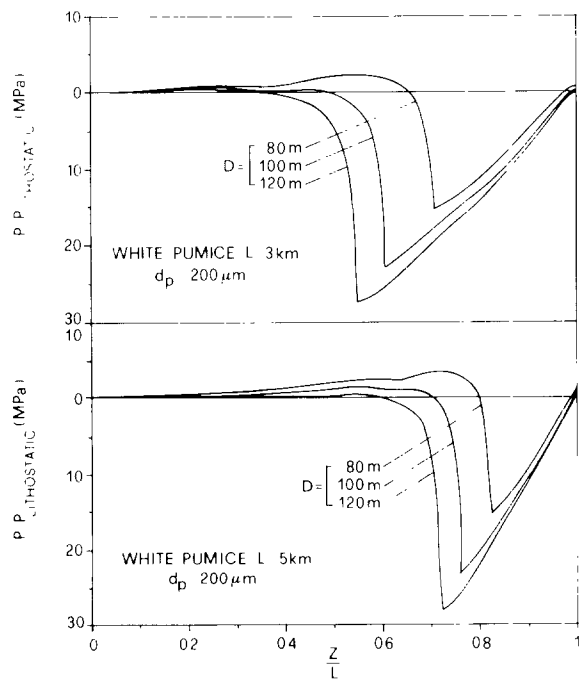

Fig. 12. Distribution of the difference between the magma and lithostatic pressure along the conduit for the white magma and particle size of 200 μm.

vius in A.D. 79 is constrained between 3 and 5 km on the basis of the studies on the thermometamorphic carbonate ejecta (Barberi and Leoni, 1980), and on equilibrium relations between the crystals present in the pumice samples and the liquids from which they originated, whose composition (see Table 1) is assumed to coincide with that of the mechanically-separated glass portion of the pumice (Barberi et al., 1981; Sigurdsson et al., 1985). For this reason, all the results presented in the paper were produced for the 3 and 5 km magma chamber depths.

The plinian eruptions produce a spectrum of particle sizes, ranging from few microns to several centimeters (Sparks and Wilson, 1976;

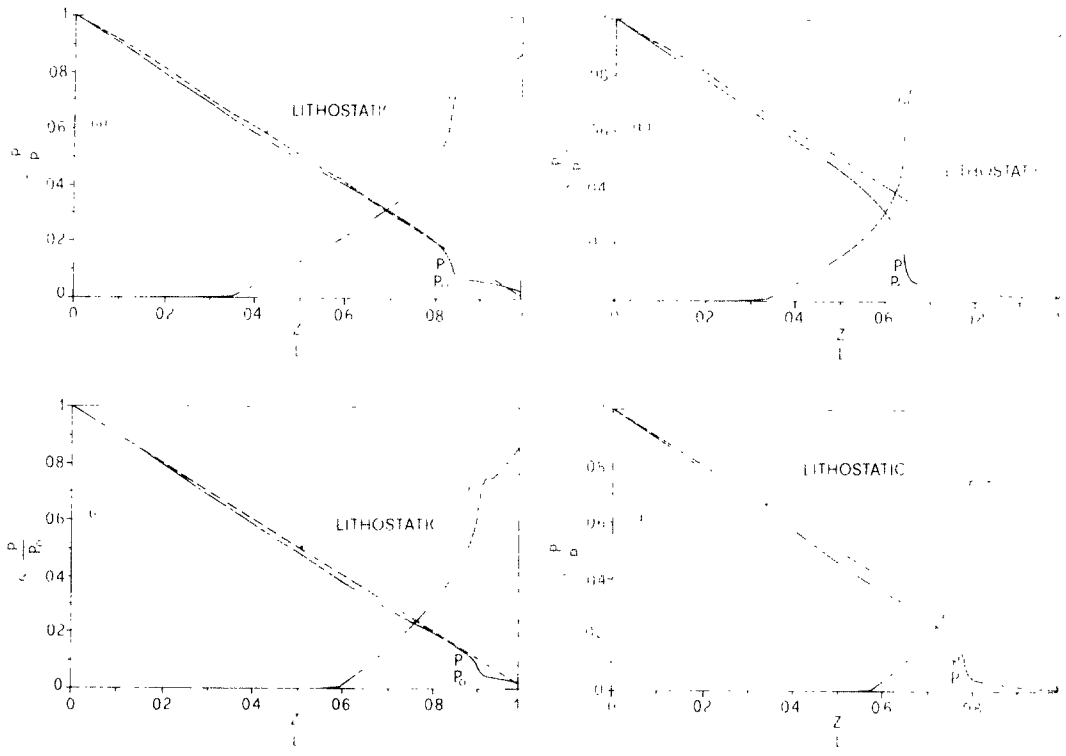

Fig. 13. Pressure and gas volumetric fraction distributions along the conduit for the gray magma and particle size of 200 μm. The dashed line corresponds to the lithostatic pressure distribution by accounting for the stratigraphy of conduit. (a) $L=3$ km, $D=80$ m; (b) $L=3$ km, $D=140$ m; (c) $L=5$ km, $D=80$ m; (d) $L=5$ km, $D=140$ m.

Walker, 1981). In the present application of the model, two different particle size classes (200 μm and 2 cm) were employed, mainly to assess the sensitivity of results on the particle diameter. A more precise modeling approach should consider a polydispersed gas-particle mixture with particle fragmentation, collisions, and relative motion with respect to the gas.

In the early simulations it was found that the effect of liquid density changes along the conduit is negligible for all considered flow conditions, and, therefore, constant magma (liquid+crystals) densities of 2400 kg/m^3 for the white magma and 2550 kg/m^3 for the gray magma were adopted in the model. It should be noted, however, that the density of magma

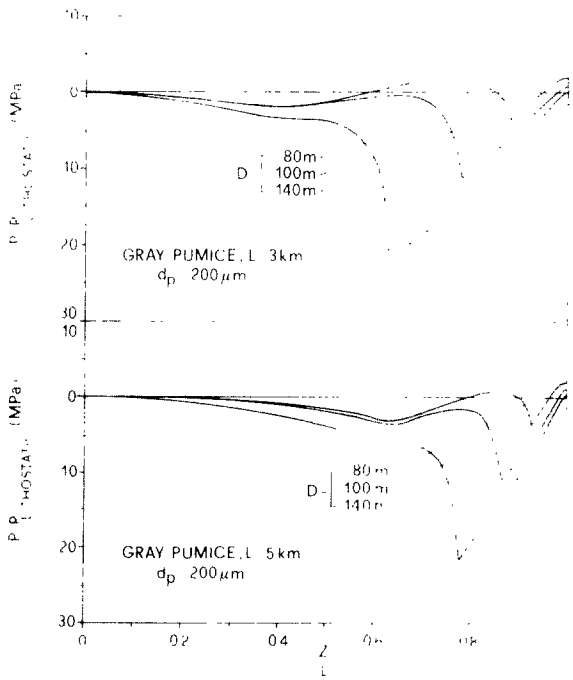

Fig. 14. Distribution of the difference between the magma and lithostatic pressure along the conduit for the gray magma and particle size of 200 μm.

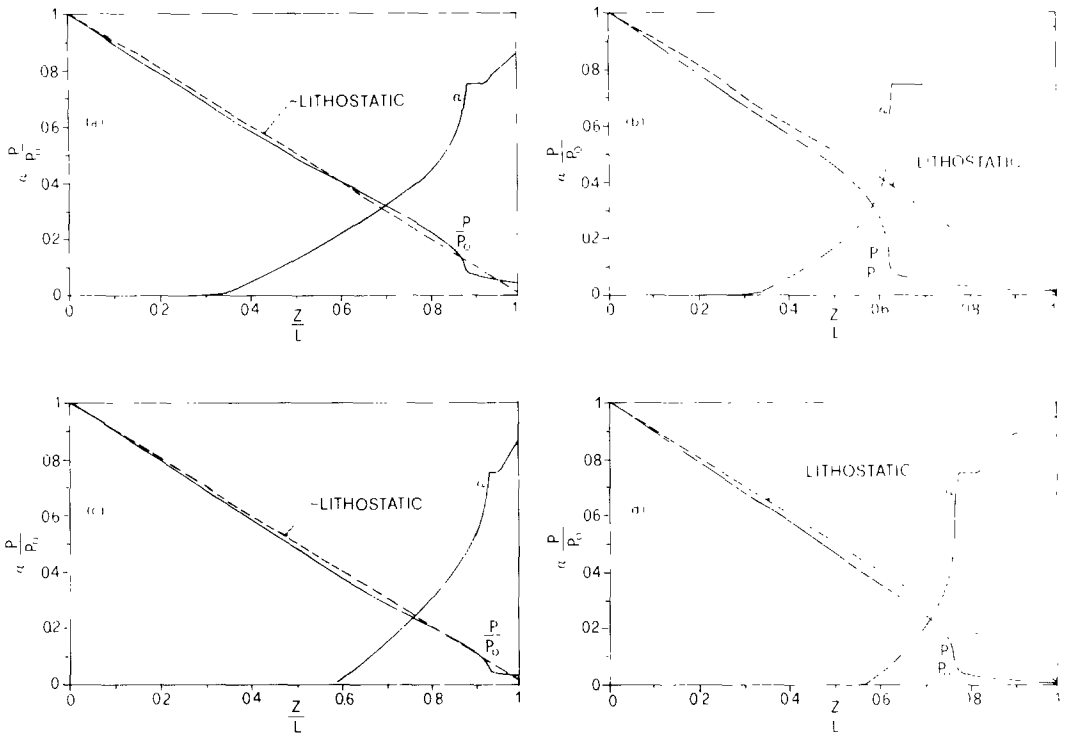

Fig. 15. Pressure and gas volumetric fraction distributions along the conduit for the gray magma and particle size of 2 cm. The dashed line corresponds to the lithostatic pressure distribution by accounting for the stratigraphy of conduit. (a) $L=3$ km, $D=80$ m; (b) $L=3$ km, $D=140$ m; (c) $L=5$ km, $D=80$ m; (d) $L=5$ km, $D=140$ m.

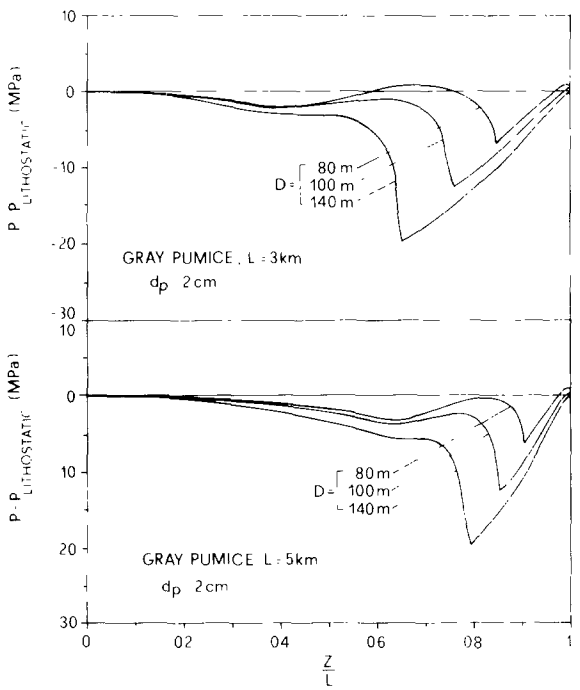

and exsolved gas is variable, both below and above the magma fragmentation zone. A constant liquid magma density favored numerical convergence and reduced the required computer time. This introduced less than 2% error in the exsolution and fragmentation levels, and less than 10% error in the viscosities which are required to produce choked-flow conditions at the conduit exit.

As discussed above, the effect of crystals on the viscosity of magma is not adequately known to be used in modeling with confidence and, therefore, we only computed the crystal-free magma viscosity and employed the ratio η_L/η_L° as an independent parameter in the model.

Fig. 16. Distribution of the difference between the magma and lithostatic pressure along the conduit for the gray magma and particle size of 2 cm.

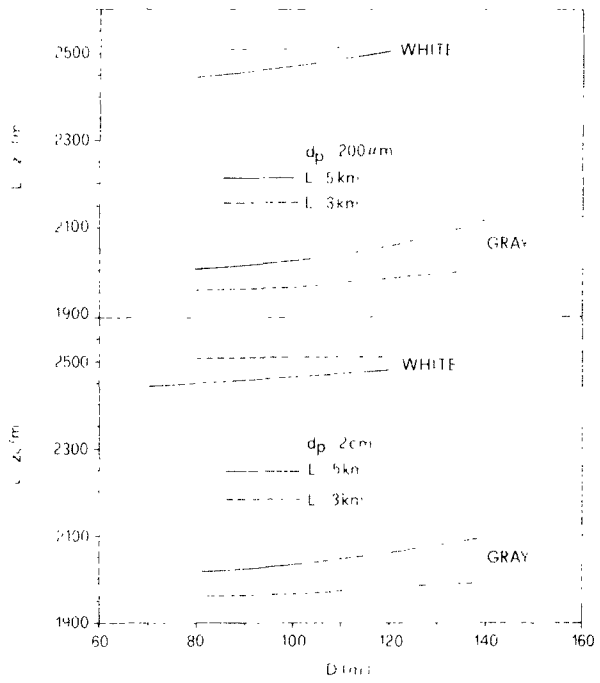

Fig. 17. The white and gray magma exsolution depth dependence with the conduit diameter for particle size of 200 μm and 2 cm, and conduit lengths of 3 and 5 km.

The parameters employed in the above non-equilibrium flow model and physical data are summarized in Table 4.

4. Results

4.1. Pressure and gas volumetric fraction variations along the conduit

The variations of pressure and gas volumetric fraction along the conduit for different conduit lengths and diameters, and particle size after the magma fragmentation level are shown in Figures 11–16. For the white magma, the results pertaining to the 2 cm particle size do not differ appreciably from those of 200 μm particle size and, therefore, are not shown.

The volumetric gas fraction in Figures 11, 13, and 15 is zero before the gas exsolution level and it shows a very rapid increase before the magma fragments at $\alpha = 0.75$. After this point α rises more slowly and attains exit values greater than 0.9. At the same time, the magma pressure decreases and, as shown in Figures 12, 14 and 16, the difference between magmatic and lithostatic pressures reaches maximum values from 15 to 30 MPa for the white and 4 to 20 MPa for the gray magma at the magma fragmentation level. These pressure differences are larger for larger conduit diameters. After the magma fragments, the rate of magma pressure decrease becomes less steep than that of the lithostatic pressure, and the mixture of gas and particles exits from the vent at a pressure above the atmospheric pressure. A major difference between the white and gray magmas is that for the former the magma pressure in the region from the magma chamber to the magma fragmentation level is greater than, or equal to, the lithostatic pressure for the considered eruption conditions (Fig. 12), whereas for the latter the magma pressure rapidly decreases below the lithostatic pressure (Figs. 14 and 16). The difference between magma and lithostatic pressures attains a maximum value between 2 and 6.5 MPa, and for the gray magma and small diameters it should be noted that this difference can become positive before the magma fragmentation zone (Figs. 14 and 16).

4.2. Exsolution and fragmentation levels

Figure 17 illustrates the depth of the exsolution level, $L - z_s$, versus the conduit diameter D for the white and gray magmas, conduit lengths of 3 and 5 km, and 2 cm and 200 μm particle size after magma fragmentation.

The white magma begins to exsolve at a depth between about 2450 and 2500 m, whereas for the gray magma this depth ranges from about 1950 to 2100 m. The exsolution depth of the gray magma is smaller than the corresponding depth of the white magma as a consequence of both its lower water content and greater solubility (see section 3.2). As can be seen from Figure 17, a shorter conduit length produces a larger exsolution depth for the white

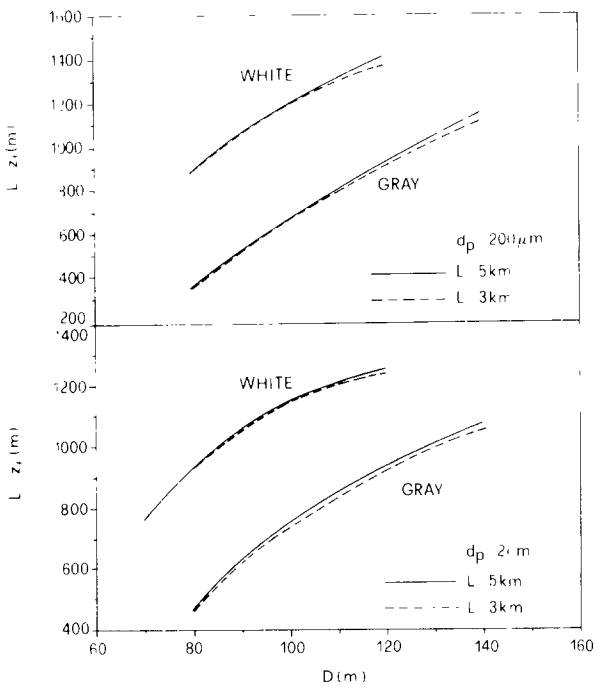

Fig. 18. The white and gray magma fragmentation depth variation with the conduit diameter for particle size of 200 μm and 2 cm, and conduit lengths of 3 and 5 km.

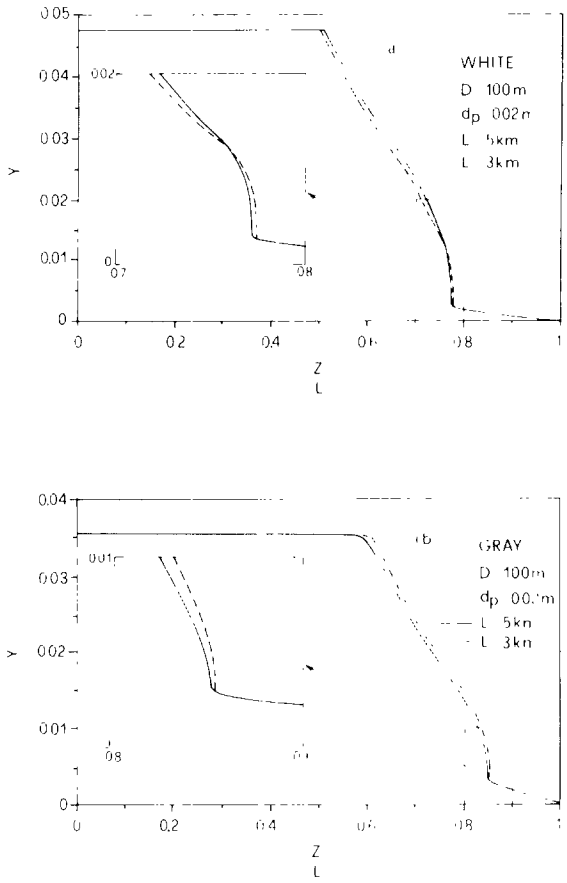

Fig. 19. Dissolved water content distribution along the conduit for the white and gray magmas, and for particle size of 2 cm and conduit diameter of 100 m.

magma and a smaller exsolution depth for the gray magma. This different effect is a consequence of the different pressure distributions within the conduit for the two magma types (see Figs. 11–16). As shown above, below the magma fragmentation level the white magma pressure is greater than lithostatic, whereas the gray magma pressure is lower than lithostatic. Because of this and the assumption that the magma chamber pressure is equal to the lithostatic pressure, the magma pressure at the conduit entrance corresponding to the 3-km conduit length is lower for the white and larger for the gray magma, than the pressure at the same depth and 5-km conduit length. Since the exsolution of water strongly depends on pressure (see section 3.2), it follows that a shorter conduit produces a larger exsolution depth in the white magma and a smaller exsolution depth in the gray magma.

Figure 18 shows the magma fragmentation depth, $L-z_f$, versus the conduit diameter D for white and gray magmas, conduit lengths of 3 and 5 km, and for particle diameters of 2 cm and 200 μm in the gas-particle flow regime. This depth is larger for the white than for the gray magma, and it increases for both magmas with increasing conduit diameters. Moreover, a shorter conduit length produces in both magmas a slightly smaller fragmentation depth. This trend is better illustrated in Figure 19 which shows the dissolved water content as a function of the nondimensional distance along the conduit z/L for both magma types and conduit lengths, conduit diameter of 100 m, and particle size of 2 cm. When the conduit length is 3 km, the larger white magma exsolution depth produces a larger viscous bubbly flow regime length than when the conduit

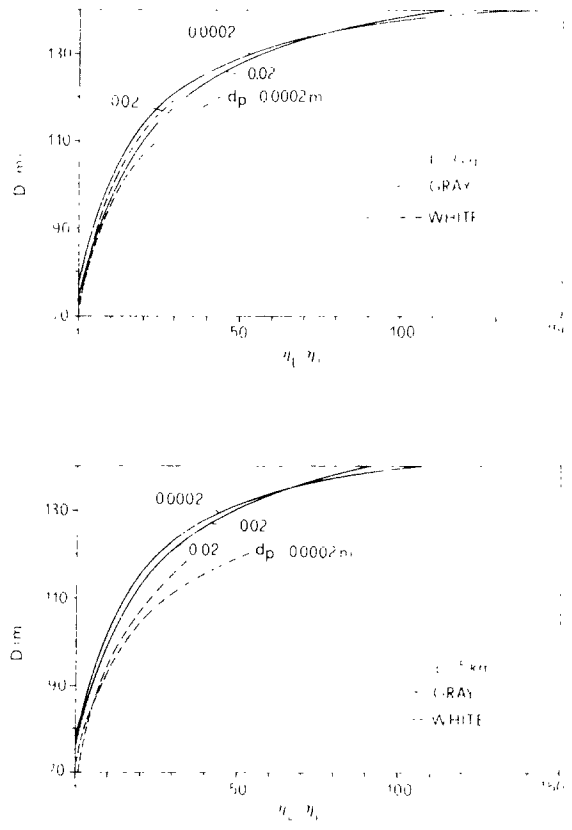

Fig. 20. Conduit diameter variation with the viscosity ratio η_L/η_L^0 for the white and the gray magma, particle diameter of 200 μm and 2 cm, and for conduit lengths of 3 and 5 km.

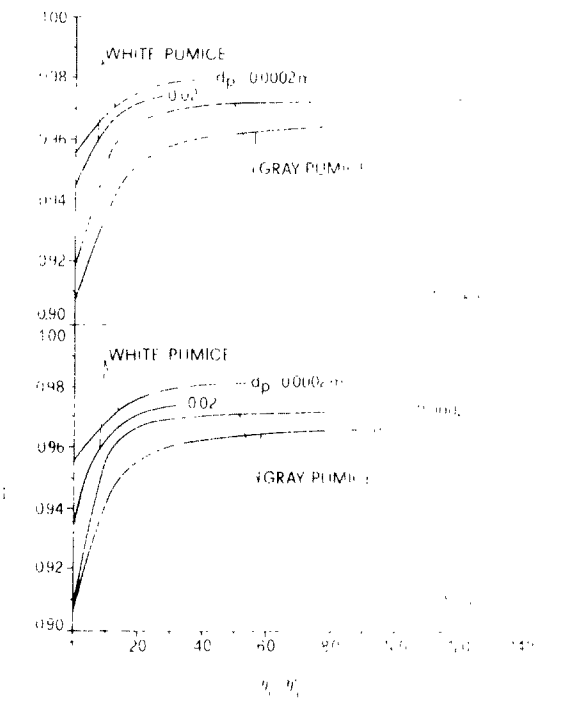

Fig. 21. Exit gas volumetric fraction distribution with the viscosity ratio η_L/η_L^0 for the white and the gray magma, particle diameter of 200 μm and 2 cm, and for conduit lengths of 3 and 5 km.

length is 5 km, and, consequently, a smaller magma viscosity is needed in order to maintain the same critical flow-rate through the conduit. On the contrary, for the gray magma the smaller exsolution depth when $L=3$ km requires a larger magma viscosity than when $L=5$ km, for a constant critical flow-rate. Thus, a larger value of viscosity is associated with L=5 km for the white magma and with $L=3$ km for the gray magma. Consequently, the pressure gradient before the magma fragments is larger for the white and smaller for the gray magma when $L=5$ km. Therefore, in all considered conditions the white magma dissolved gas mass fraction distributions for 3 and 5 km cross each other (as shown in the enlargement of Fig. 19a) and produce a smaller fragmentation depth for $L=3$ km. For the considered conditions in Table 4, no such crossover of the gray magma dissolved gas mass fraction occurs (Fig. 19b) and the fragmentation depth is also smaller for a smaller conduit length.

4.3. *Exit conditions*

The variations of conduit diameter, exit gas volumetric fraction, exit pressure, and gas and particle exit velocities are illustrated in Figures 20–23 as a function of the viscosity ratio η_L/η_L^0 for white and gray magmas, conduit lengths of 3 and 5 km, and particle size of 2 cm and 200 μm.

As expected, the conduit diameter increases with magma viscosity at fixed critical flow-rates for both magmas (Fig. 20). At a constant η_L/η_L^0 the conduit diameter is larger for the gray than for the white magma for almost all considered conditions, with the difference increasing with the conduit length. Since the crystal volumetric fraction is similar for the two

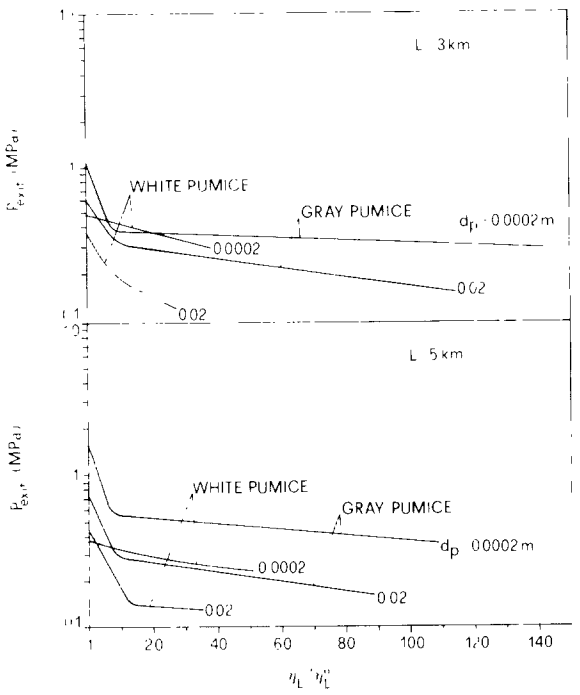

Fig. 22. Exit pressure distribution with the viscosity ratio η_L/η_L^0 for the white and the gray magma, particle diameter of 200 μm and 2 cm, and for conduit lengths of 3 and 5 km.

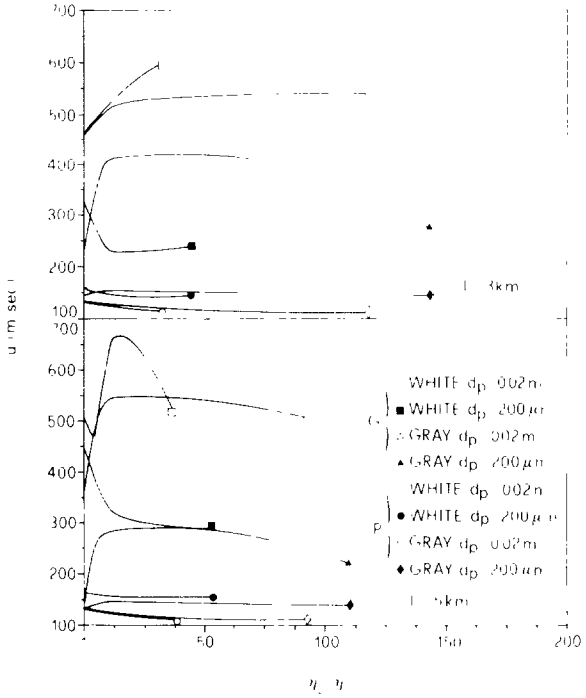

Fig. 23. Exit gas (G) and particle (P) velocity distributions with the viscosity ratio η_L/η_L^0 for the white and the gray magma, particle diameter of 200 μm and 2 cm, and for conduit lengths of 3 and 5 km.

magma types (see Table 3), this implies a vent widening from the white to the gray pumice eruption phases. Such an enlargement of the conduit diameter with time is proposed by Sheridan et al. (1981) as the consequence of an increasing vent erosion due to the larger "explosivity" of the gray magma phase. This is also suggested by Carey and Sigurdsson (1987) to explain an increasing discharge rate with time as inferred by the granulometric studies of the deposit. As shown in Figure 20, the particle size has a larger effect on the conduit diameter for the white than for the gray magma, with the effect on the diameter being less than 6 m.

Figure 21 shows the exit gas volumetric fraction or exit void fraction as a function of the viscosity ratio η_L/η_L^0. The void fraction is greater for the white than for the gray magma, and it increases rapidly for small viscosity ratios and thus with conduit diameters (see Fig. 20). A reduction of the particle diameter from 2 cm to 200 μm produces a further increase of void fraction, whereas the conduit length has only a minor effect.

The exit pressure distribution with viscosity shown in Figure 22 is significantly higher for the gray than for the white magma, except for shorter conduits, smaller particle sizes, and viscosity ratios of about 10 where the two pressures are nearly equal. In other cases this pressure difference ranges from 0.2 to 1 MPa. It should be noted, however, that in our calculations no account was taken of the existence of a crater which has the effect of reducing the exit pressure and accelerating the gas- particle mixture. Smaller particles produce a larger exit pressure, whereas a shorter conduit significantly reduces the exit pressure for gray magma and particle size of 200 μm, according to the very high viscosity associated with these conditions (see also Fig. 20).

The exit velocities of gas and particles are shown in Figure 23. The gas velocity is higher

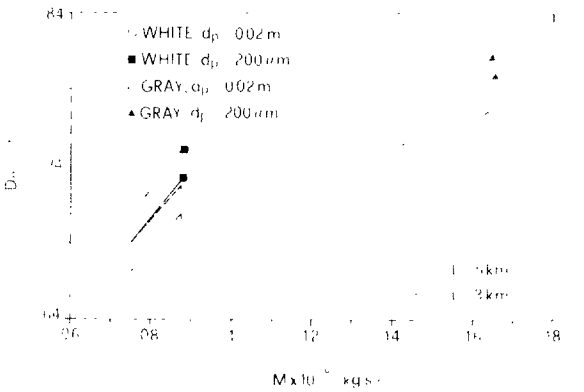

Fig. 24. Variation of the minimum conduit diameter with the magma mass discharge rate for the white and the gray magma, particle diameter of 200 μm and 2 cm, and for conduit lengths of 3 and 5 km.

for a larger particle size as a consequence of the reduced interfacial drag between the phases. In this case the exit velocities range from 400 to 700 m/s for the gas and from 110 to 130 m/s for the particles, for both magma types. The smaller particles reduce significantly the gas exit velocity because of the increased drag between the phases; the gas velocity ranges from 180 to 400 m/s whereas the particle velocity remains at about 150 m/s for all considered conditions.

5. Discussion

The magma flow model predicts the existence of a minimum conduit diameter for a maximum or choked flow-rate. This minimum diameter corresponds to the viscosity ratio $\eta_L/\eta_L^0 = 1$. A decrease of the diameter below its minimum, for the same mass flow-rate, would lead to a choked flow inside the conduit which would then require an increase of the diameter above the choked flow position in the conduit (Wilson and Head, 1981; Buresti and Casarosa, 1989). Figure 24 illustrates the minimum conduit diameter as a function of magma discharge rate, for both the white and gray magma, conduit lengths of 3 and 5 km, and particle size of 2 cm and 200 μm. For the white

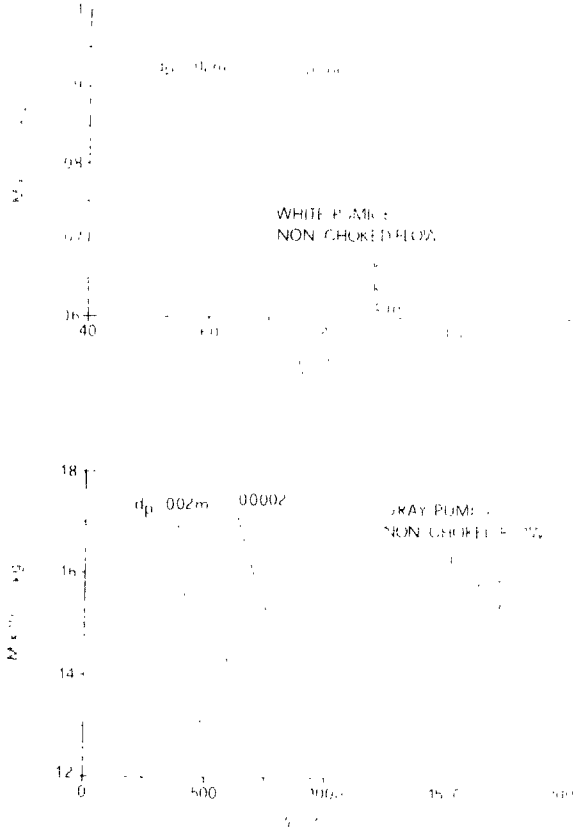

Fig. 25. Magma mass discharge rate dependence with viscosity ratio η_L/η_L^0 for the non-choked flow condition in conduit and exit pressure equal to atmospheric. The curves correspond to particle size of 200 μm and 2 cm, conduit lengths of 3 and 5 km, and to the conduit diameter of 140 m for the white magma and 200 m for the gray magma.

pumice eruption phase corresponding to $M = 8 \times 10^7$ kg/s, the minimum conduit diameter ranges from 69 to 72 m and is larger for smaller conduit lengths and particle size. For the gray pumice eruption phase with $M = 1.5 \times 10^8$ kg/s, the minimum conduit diameter ranges from 73 to 79 m and is larger for longer conduits and smaller particles. The different effect of a shorter conduit length on the minimum diameter of the white and gray magmas is again tied to the different pressure distribution within the conduit as shown in Figures 11–16.

For a given magma flow-rate through a conduit and atmospheric pressure near the conduit exit, the conduit length and magma char-

acteristics determine the conduit diameter. When the flow in the conduit becomes maximum or choked, the diameter cannot be larger than a critical value which corresponds to the exit pressure being close to the atmospheric pressure. A conduit with a diameter above this maximum cannot anymore sustain a choked flow condition and the flow-rate becomes subcritical. The results in Figure 25 depict the magma flow-rate distribution with the crystal viscosity ratio for the non-choked flow conditions, white and gray magma, exit pressure corresponding to atmospheric, different conduit lengths and particle sizes, and for conduit diameters of 140 m for the white and 200 m for the gray magma. These results, therefore, provide the maximum possible values of viscosity ratios for a given magma discharge rate consistent with the considered diameters. For these conduit diameters and mass flow rates of 8×10^7 kg/s for the white magma, and 1.5×10^8 kg/s for the gray magma, the corresponding viscosity ratios are 90 and 1100, respectively. By comparing these values with those in Figure 9, with the crystal volumetric fraction as given in Table 3 for two magma types, it follows that the use of the Sherman's crystal viscosity relation leads to very large conduit diameters and non-choked flow condition. There is, however, an evidence that the exit pressures of fragmented magmas of real eruptions are larger than atmospheric, and that the mixtures of gas and particles exit from the vents at supersonic speeds and interact with the atmosphere through complex systems of shocks (Kieffer, 1981). This implies that the critical flow conditions are commonly reached within the conduits. Hence, the crystal viscosity ratios given in Figure 9a are more reliable than those given by the Sherman's relation, since they are consistent with the choked-flow conditions. By considering the crystal volume fractions of white and gray magmas prior to the eruption (see section 3.4 and Table 3), it follows that the value of the viscosity ratio is in the range between 2 and 8 for both magma types (Fig. 9a). This range is consistent with a conduit diameter between 70 and 90 m for the white magma, and between 75 and 100 m for the gray magma (Fig. 20). It should be noted from Figure 20 that for some combination of particle size and conduit length the model predicts no conduit enlargement from the white to the gray eruption phase. This behavior can be explained by considering the total mass flow-rate expression:

$$M=A[\rho_G u_G \alpha+\rho_L u_L(1-\alpha)] \tag{33}$$

and noting that the gas mass flow-rate in this equation is about five orders of magnitude smaller than the particle mass flow-rate for the considered eruptive conditions. If we now assume that no conduit enlargement takes place and note from Figure 23 that the exit particle velocities are nearly equal for the white and gray magma, we obtain from the above equation:

$$\frac{M^{GM}}{M^{WM}}\approx\frac{(1-\alpha^{GM})\rho_L^{GM}}{(1-\alpha^{WM})\rho_L^{WM}} \tag{34}$$

where the superscripts GM and WM refer to gray and white magma, respectively. Using the void fractions from Figure 21 with a crystal viscosity ratio between 2 and 8 as discussed above (i.e., $\alpha=0.93$ for gray and $\alpha=0.96$ for white magma) and the densities of the two degassed liquids as computed in section 3.4 ($\rho_L^{GM}=2650$ kg/m^3 and $\rho_L^{WM}=2565$ kg/m^3) it is obtained that $M^{GM}/M^{WM}=1.81$, which is very similar to the mass flow-rate ratio $1.5\times10^8/8\times10^7=1.87$. Thus, an increase with time of the discharge rate during the A.D. 79 eruption of Vesuvius, as inferred from the field studies on the dispersal of the fallout deposit and on its grain size characteristics (Carey and Sigurdsson, 1987; Sigurdsson et al., 1990), is consistent with either a progressive widening of the conduit or the tapping of a magma which

is progressively less rich in volatiles at a constant conduit diameter. However, an enlargement of conduit with time is also suggested by the pressure distribution within the conduit for the two magma types. This enlargement can be precipitated by a change in the magma composition from white to gray whereby the pressure in the deeper region of conduit is decreased below lithostatic (Figs. 11–16), which may cause the conduit wall collapse. Such a wall collapse process can then explain an increasing lithic content in the fallout deposit from white to gray pumice, with a significantly larger proportion of deep limestone fragments (Lirer et al., 1973). In addition, the higher exit pressure of the gray magma can also produce a more efficient vent erosion. The maximum conduit wall erosion appears to be located near the magma fragmentation region, where both the difference between the lithostatic and magma pressure (see Figs. 11–16) and the two-phase mixture viscosity are maximized (Dobran, 1992; Macedonio et al., 1994). This implies that the most abundant lithics in the deposits should be removed from a region between 500 and 1500 m depth (Fig. 18), and thus they should consist of tephritic lavas, sandstones, and tuffites (see Fig. 2), which is in accord with data of Barberi et al. (1989).

A higher lithic content, when combined with a lower exit void fraction of gray magma than of white magma (Fig. 21), produces a denser column which can lead to local instabilities and partial column collapses, or to the formation of fountains and radially spreading pyroclastic flows (Dobran et al., 1994). This is consistent with reconstructed events of the A.D. 79 gray eruption phase of Vesuvius which produced surges that destroyed Hercolaneum and Pompei, and a total column collapse leading to the deposition of a lithic-rich pumice flow (Sigurdsson et al., 1985, 1990; Carey and Sigurdsson, 1987; Barberi et al., 1989).

The magma pressure decrease below the lithostatic in deeper regions of the conduit during the gray eruption phase is also consistent with the later stages of the eruption when magma–water interaction took place (Sigurdsson et al., 1985; Barberi et al., 1989). Sheridan et al. (1981) found that the occurrence of an important phreatomagmatic phase in explosive eruptions of Somma-Vesuvius is associated with a magma chamber below the carbonate basement level. They also found that those eruptions which are characterized by a strong hydromagmatic activity have a strong concentration of carbonate lithics in the deposit immediately below the surge beds. These observations suggest that no important aquifer existed in the uppermost 2000 m below the volcano (as also found from the geothermal drilling by Balducci et al., 1985), and point out to a link between water inflow into the conduit and presence of lithics of deep provenance, which is also suggested by Barberi et al. (1988). However, Barberi et al. (1989) argue that no explosive interaction can take place before magma fragments, because of the insufficient surface area for a rapid heat transfer, implying that an explosive magma–water interaction cannot take place at the carbonate basement level. This conclusion should not, however, be interpreted that an interaction of nonfragmented magma with water cannot produce an explosive interaction; such an interaction may produce stress waves, for example, causing brittle fracture or vesiculation in the melt and a fragmentation of magma leading to a subsequent explosive interaction with water (Dobran et al., 1990).

6. Summary and Conclusions

The magma ascent during the A.D. 79 eruption of Vesuvius was studied by a one-dimensional, isothermal, and steady-state two-phase flow model which accounts for the relative velocity between the phases, and for variable magma density and viscosity. By considering water as the only gas phase, the gas exsolution

process was modeled by assuming chemical equilibrium between the dissolved and exsolved gas. This model provides an explanation for the observed water contents in the two magma types. The magma viscosity was modeled according to Shaw (1972) and the crystal contribution to viscosity was considered as a parameter in the simulations in order to place constraints on the crystal viscosity relations based on the crystal contents of white and gray magmas. The magma density was computed by a model equation of Lange and Carmichael (1987) and by accounting for the effect of crystal content. The exsolution, viscosity, and density models take into consideration the different compositions of white and gray magmas.

The input information to the model involved the magma mass flow- rate, conduit geometry, stratigraphy of rocks, and magma composition. By taking the magma flow-rate as the maximum flow which is consistent with the conduit geometry and magma composition, the two-phase flow parameters along the conduit were then established by the model.

For all considered eruption conditions, the magma pressure in the conduit decreases below the lithostatic pressure near the magma fragmentation level. This pressure difference attains values between 4 and 30 MPa for different magma compositions, conduit lengths, particle size after magma fragmentation, and it increases with conduit diameters. The pressure distributions in the deep conduit regions vary with the magma compositions, being larger than lithostatic for the white and smaller than lithostatic for the gray magma.

The exsolution and fragmentation levels in the conduit are deeper for the white than for the gray magma as a consequence of the greater solubility and lower water content of the latter magma. The effect of the changing magma composition during the eruption is to increase the exit pressure and decrease the exit gas volumetric fraction. The model predictions are also consistent with an increasing conduit diameter during the eruption, for almost all of the considered conditions.

The model of the magma flow through the conduit of the A.D. 79 eruption of Vesuvius predicts the existence of a minimum conduit diameter which is consistent with the white and gray magma compositions and mass flow-rates. This minimum diameter is about 70 m for the white and about 75 m for the gray magma. Furthermore, the use of the Einstein-derived crystal viscosity relations appears to be more reliable than that of Sherman because it is consistent with the choked flow conditions at the conduit. This implies a conduit diameter from 70 to 90 m for the white and from 75 to 100 m for the gray magma.

The predictions of the model are consistent with column collapses during the gray eruption phase and with a large presence of carbonate lithics in the gray pumice fall deposit, as well as with an interaction with water during a late stage of the eruption.

Acknowledgment

This work was partially supported by the Gruppo Nazionale per la Vulcanologia, Italy.

Nomenclature

a	activity
A	conduit cross-sectional area
B_1, B_2	constants in Eqn. (3)
C_p	specific heat at constant pressure
d_C	crystal diameter
d_p	particle diameter
D	conduit diameter
f	fugacity
f_F	friction coefficient
F	drag force
g	gravitational acceleration
G	mass flux, M/A
h	depth below the surface
k	coefficient in Eqns. (17) and (18)
K	conduit entrance loss coefficient
L	conduit length
m	molecular weight
M	mass flow-rate

n	total number of components in magma
P	pressure
R	gas constant
Re	Reynolds number
$\bar{R}$	coefficient defined in Eqn. (25)
T	temperature
u	velocity of gas or magma
V	molar volume
$\bar{V}$	partial molar volume
Ve	vesiculation
w	symmetric binary interaction parameter
x	molar fraction of component in magma
Λ	exsolved gas mass fraction
Y	dissolved gas mass fraction in liquid
W	crystal mass fraction in liquid
z	vertical coordinate, see Fig. 1

Greek

α	gas volumetric fraction
η	viscosity
ϑ	defined in Eqn. (20)
μ	chemical potential
ξ	wetted perimeter
ρ	density
ϕ	crystal volume fraction

Subscripts

atm	atmosphere
B	bottom
c	country rock
f	fragmentation
G	gas
H	hydraulic
L	liquid magma or particles after fragmentation
Li	ith crystal in liquid
Lo	crystal-free liquid
M	magma chamber
min	minimum
o	stagnation state in magma chamber
P	pumice
Pi	ith crystal in pumice
ref	reference
s	exsolution
T	top
w	conduit or magma chamber wall

Superscripts

G	gas
GM	gray magma
L	liquid
WM	white magma

References

Balducci, S., Vaselli, M. and Verdiani, G., 1983. Exploration well in the "Ottaviano" permit, Italy. In: K.S. Strub and P. Ungemach (Editors), European Geothermal Update. Proc. 3rd Int. Seminar on the Results of the EC Geothermal Energy Research, Munich (1983). D. Reidel, Dordrecht, pp. 407–418.

Barberi, F. and Leoni, L., 1980. Metamorphic carbonate ejecta from Vesuvius plinian eruptions. Evidence of the occurrence of shallow magma chambers. Bull. Volcanol., 43: 107–120.

Barberi, F., Bizouard, H., Clocchiatti, R., Metrich, N., Santacroce, R. and Sbrana, A., 1981. The Somma-Vesuvius magma chamber: a petrological and volcanological approach. Bull. Volcanol., 44: 295–315.

Barberi, F., Navarro, J.M., Rosi, M., Santacroce, R. and Sbrana, A., 1988. Explosive interaction of magma with ground water: insights from xenoliths and geothermal drillings. Rend. Soc. Ital. Mineral. Petrol., 43: 961–976.

Barberi, F., Cioni, R., Rosi, M., Santacroce, R., Sbrana, A. and Vecci, R., 1989. Magmatic and phreatomagmatic phases in explosive eruptions of Vesuvius as deduced by grain-size and component analysis of the pyroclastic deposits. J. Volcanol. Geotherm. Res., 38: 287–307.

Bondi, A., 1967. Viscosity and molecular structure. In: F.R. Eirich (Editor), Rheology, 4. Academic Press, New York, NY, pp. 1–83.

Bottinga, Y. and Weill, D.F., 1972. The viscosity of magmatic silicate liquids: a model for calculation. Am. J. Sci., 272: 438–475.

Buresti, G. and Casarosa, C., 1989. One-dimensional adiabatic flow of equilibrium gas-particle mixtures in long vertical ducts with friction. J. Fluid Mech., 203: 251–272.

Burnham, C.W. and Davis, N.F., 1974. The role of H_2O in silicate melts: II. Thermodynamic and phase relations in the system $NaAlSi_3O_8$-H_2O to 10 kilobars, 700° to 1100° C. Am. J. Sci., 274: 902–940.

Burnham, C.W. and Jahns, R.H., 1962. A method for determining the solubility of water in silicate melts. Am. J. Sci., 260: 721–745.

Carey, S. and Sigurdsson, H., 1987. Temporal variations in column height and magma discharge rate during the 79 AD eruption of Vesuvius. Geol. Soc. Am. Bull., 99: 303–314.

Carmichael, I.S.E., Nicholls, J., Spera, F.J., Wood, B.J. and Nelson, S.A., 1977. High temperature properties of silicate liquids: applications to the equilibration and ascent of basic magma. Philos. Trans. R. Soc. London Ser. A, 286: 373–431.

Civetta, L., Galati, R. and Santacroce, R., 1991. Magma mixing and convective compositional layering within

the Vesuvius magma chamber. Bull. Volcanol., 53: 287–300.

Clayton, W., 1954. The Theory of Emulsions and their Technical Treatment. 5th ed. by C.G. Sumner. The Blakiston Company, New York.

Cornell, W. and Sigurdsson, H., 1987. Compositional zoning in the Pompei 79 AD pumice deposit: magma mixing and observed trends. Eos, 68: 434.

Deer, W.A., Howie, R.A. and Zussman, J., 1962. Rock-Forming Minerals. Vol. Three: Sheet Silicates. Longmans, Green and Co. Ltd., London.

Dingwell, D.B., Harris, D.M. and Scarfe, C.M., 1984. The solubilty of H_2O in melts in the system SiO_2-Al_2O_3-Na_2O-K_2O at 1 to 2 kbars. J. Geol., 92: 387–395.

Dobran, F., 1992. Nonequilibrium flow in volcanic conduits and application to the eruptions of Mt. St. Helens on May 18, 1980, and Vesuvius in AD 79. J. Volcanol. Geotherm. Res., 49: 285–311.

Dobran, F. and Papale, P., 1992. CONDUIT2: A computer program for modeling steady-state two-phase flows in volcanic conduits. VSG Rep. No. 92-5, Giardini, Pisa.

Dobran, F., Barberi, F. and Casarosa, C., 1990. Modeling of volcanological processes and simulation of volcanic eruptions. CNR-GNV Rep. VSG90-01, Giardini, Pisa.

Dobran, F., Neri, A. and Macedonio, G., 1993. Numerical simulation of collapsing volcanic columns. J. Geophys. Res., 98: 4231–4259.

Eggler, D.H. and Burnham, W., 1984. Solution of H_2O in diopside melts: A thermodynamic model. Contrib. Mineral. Petrol., 85: 58–66.

Epel'baum, M.B., 1985. The structure and properties of hydrous granitic melts. Geol. Carpathica, 36: 491–498.

Ghiorso, M.S. and Carmichael, I.S.E., 1980. A regular solution model for met-aluminous silicate liquids: applications to geothermometry, immiscibility, and the source regions of basic magma. Contrib. Mineral. Petrol., 71: 323–342.

Ghiorso, M.S., Carmichael, I.S.E., Rivers, M.L. and Sack, R.O., 1983. The Gibbs free energy of mixing of natural silicate liquids; an expanded regular solution approximation for the calculation of magmatic intensive variables. Contrib. Mineral. Petrol., 84: 107–145.

Hamilton, D.L., Burnham, C.W. and Osborn, E.F., 1964. The solubility of water and effects of oxygen fugacity and water content on crystallization in mafic magmas. J. Petrol., 5, Part 1: 21–39.

Harr, L., Gallagher, S. and Kell, G.S., 1984. Steam Tables. Hemisphere, Washington DC.

Hodges, F.N., 1974. The solubility of H_2O in silicate melts. Year Book Carnegie Inst. Washington, 73: 251–255.

Ishii, M. and Zuber, N., 1979. Drag coefficient and relative velocity in bubbly, droplet and particulate flows. AIChE J., 25: 843–855.

Kieffer, S.W., 1981. Blast dynamics of Mt. St. Helens on May. 18, 1980. Nature, 291: 568–571.

Kogarko, L.N., Burnham, C. and Shettle, D., 1977. Water regime in alkalic magmas. Geokhimiya, 5: 643–651.

Kushiro, I., 1976. Changes in viscosity and structure of melt of $NaAlSi_2O_6$ composition at high pressures. J. Geophys. Res., 81: 6347–6350.

Kushiro, I., 1978. Viscosity and structural changes of albite ($NaAlSi_3O_8$) melt at high pressures. Earth Planet. Sci. Let., 41: 87–91.

Kushiro, I., 1981. Viscosity change with pressure of melts in the system CaO-Al_2O_3-SiO_2. Year Book Carnegie Inst. Washington, 80: 339–341.

Kushiro, I., 1986. Viscosity of partial melts in the upper mantle. J. Geophys. Res., 91: 9343–9350.

Lange, R.A. and Carmichael, I.S.E., 1987. Densities of Na_2O-K_2O-CaO-MgO-FeO-Fe_2O_3-Al_2O_3-TiO_2-SiO_2 liquids: New measurements and derived partial molar properties. Geochim. Cosmochim. Acta, 51: 2931–2946.

Lirer, L., Pescatore, T., Booth, B. and Walker, G.P.L., 1973. Two plinian pumice-fall deposits from Somma-Vesuvius, Italy. Geol. Soc. Am. Bull., 84: 759–772.

Lowell, R.P., 1985. Double-diffusive convection in partially molten silicate systems: Its role during magma production and in magma chambers. J. Volcanol. Geotherm. Res., 26: 1–24.

Macedonio, G., Dobran, F. and Neri, A., 1994. Erosion processes in volcanic conduits and application to Vesuvius. Earth Planet. Sci. Lett., 121, in press.

Manning, D.A.C., Hamilton, C.M.B., Henderson, C.M.B. and Dempsey, M.J., 1980. The probable occurrence of interstitial Al in hydrous F-bearing and F-free aluminosilicate melts. Contrib. Mineral. Petrol., 75: 257–262.

Marsh, B.D., 1981. On the crystallinity, probability of occurrence, and rheology of lava and magma. Contrib. Mineral. Petrol., 78: 85–98.

McBirney, A.R. and Murase, T., 1984. Rheological properties of magmas. Annu. Rev. Earth. Planet. Sci., 12: 337–357.

McBirney, A.R., Baker, B.H. and Nilson, R.H., 1985. Liquid fractionation. Part I: Basic principles and experimental simulations. J. Volcanol. Geotherm. Res., 24: 1–24.

McMillan, P. and Holloway, J., 1987. Water solubility in aluminosilicate melts. Contrib. Mineral. Petrol., 97: 320–332.

McMillan, P., Peraudeau, G., Holloway, J. and Coutures, J.P., 1986. Water solubility in a calcium aluminosilicate melts. Contrib. Mineral. Petrol., 94: 178–182.

Modell, M. and Reid, R.C., 1974. Thermodynamics and its Applications. Prentice Hall, Englewood Cliffs, NJ, 553 pp.

Murase, T. and McBirney, A.R., 1973. Properties of some common igneous rocks and their melts at high temper-

atures. Geol. Soc. Am. Bull., 84: 3563–3592.
Murase, T., McBirney, A.R. and Melson, W.G., 1985. Viscosity of the dome of Mount St. Helens. J. Volcanol. Geotherm. Res., 24: 193–204.
Mysen, B.O., 1988. Structure and Properties of Silicate Melts. Developments in Geochemistry 4. Elsevier Amsterdam.
Mysen, B.O. and Virgo, D., 1986. Volatile in silicate melts at high pressure and temperature. 1. Interaction between OH groups and Si^{4+}, Al^{3+}, Ca^{2+} Na^{+} and H^{+}. Chem. Geol., 57: 303–331.
Mysen, B.O., Virgo, D., Harrison, W.J. and Scarfe, C.M., 1980. Solubility mechanisms of H_2O in silicate melts at high pressures and temperatures: A Raman spectroscopic study. Am. Mineral., 65: 900–914.
Nelson, S.A. and Carmichael, I.S.E., 1979. Partial molar volumes of oxide components in silicate liquids. Contrib. Mineral. Petrol., 71: 117–124.
Nicholls, J., 1980. A simple thermodynamic model for estimating the solubility of H_2O in magmas. Contrib Mineral. Petrol., 74: 211–220.
Nilson, R.H., McBirney, A.R. and Baker, B.H., 1985. Liquid fractionation. Part II: Fluid dynamics and quantitative implications for magmatic systems. J. Volcanol. Geotherm. Res., 24: 25–54.
Oxtoby, S. and Hamilton, D.L., 1978. The discrete association of water with Na_2O and SiO_2 in Na-Al silicate melts. Contrib. Mineral. Petrol., 66: 185–188.
Remmele, R., Stanton, T., McMillan, P. and Holloway, J., 1986. Raman spectra of hydrous glasses along the quartz-albite join (abstract). EOS, 67: 1274
Russell, L.E., 1957. Solubility of water in molten glass. J. Soc. Glass Technol., 41: 304T–317T.
Santacroce, R., 1987. Somma-Vesuvius. Quaderni de "La Ricerca Scientifica", CNR-114, Vol. 8, Roma.
Scarfe, C.M., 1981. The pressure dependence of the viscosity of some basic melts. Year Book Carnegie Inst. Washington, 80: 336–339.
Shaw, H.R., 1965. Comments on viscosity, crystal settling and convection in granitic magmas. Am. J. Sci., 273: 120–152.
Shaw, H.R., 1972. Viscosities of magmatic silicate liquids: an empirical method of prediction. Am. J. Sci., 272: 870–893.
Shaw, H.R., 1974. Diffusion of H_2O in granitic liquids: Part I. Experimental data; Part II. Mass transfer in magma chambers. In: A.W. Hoffman, and others (Editors), Geochemical Transport and Kinetics. Carnegie Inst. Washington Publ., 634: 139–170.
Sheridan, M.F. and Wohletz, K.H., 1983. Hydrovolcanism: basic considerations and review. J. Volcanol. Geotherm. Res., 17: 1–29.
Sheridan, M.F., Barberi, F., Rosi, M. and Santacroce, R., 1981. A model for Plinian eruptions of Vesuvius. Nature, 289: 282–285.
Sherman, P., 1968. Emulsion Science. Academic Press, New York, NY.
Sigurdsson, H., Cashdollar, S. and Sparks, R.S.J., 1982. The eruption of Vesuvius in AD 79: reconstruction from historical and volcanological evidence. Am. J. Archaeol., 86: 39–51.
Sigurdsson, H., Carey, S., Cornell, W. and Pescatore, T., 1985. The eruption of Vesuvius in 79 AD. Nat. Geogr. Res., 1: 332–387.
Sigurdsson, H., Cornell, W. and Carey, S., 1990. Influence of magma withdrawal on compositional gradients during the AD 79 Vesuvius eruption. Nature, 345: 519–521.
Silver, L. and Stolper, E., 1985. A thermodynamic model for hydrous silicate melts. J. Geol., 93: 161–178.
Silver, L.A., Ihinger, P.D. and Stolper, E., 1990. The influence of bulk composition on the speciation of water in silicate glasses. Contrib. Mineral. Petrol., 104: 142–162.
Sparks, R.S.J., 1978. The dynamics of bubble formation and growth in magmas: a review and analysis. J. Volcanol. Geotherm. Res., 3: 1–37.
Sparks, R.S.J. and Wilson, L., 1976. A model for the formation of ignimbrite by gravitational column collapse. J. Geol. Soc. London, 132: 441–451.
Spera, F.J., Yuen, D.A. and Kemp, D.V., 1984. Mass transfer rates along vertical wall in magma chambers and marginal upwelling. Nature, 310: 764–767.
Stolper, E.M., 1982a. Water in silicate glasses: An infrared spectroscopic study. Contrib. Mineral. Petrol., 81: 1–17.
Stolper, E.M., 1982b. The speciation of water in silicate melts. Geochim. Cosmochim. Acta, 46: 2609–2620.
Tomlinson, J.W., 1956. A note on the solubility of water in molten sodium silicate. J. Soc. Glass Technol., 40: 25T–31T.
Trial, A.F. and Spera, F.J., 1988. Natural convection boundary layer flows in isothermal ternary systems: Role of diffusive coupling. Int. J. Heat Mass Transf., 31: 941–955.
Trial, A.F. and Spera, F.J., 1990. Mechanisms for the generation of compositional heterogeneities in magma chambers. Geol. Soc. Am. Bull., 102: 353–367.
Tuttle, O.F. and Bowen, N.L., 1958. Origin of granite in the light of experimental studies in the system $NaAlSi_3O_8$-$KAlSi_3O_8$-SiO_2-H_2O. Geol. Soc. Am. Mem., 74.
Walker, G.P.L., 1981. Plinian eruptions and their products. Bull. Volcanol., 44: 223–240.
Wilson, L. and Head III, J.W., 1981. Ascent and eruption of basaltic magma on the earth and moon. J. Geophys. Res., 86: 2971–3001.
Wilson, L., Sparks, R.S.J. and Walker, G.P.L., 1980. Explosive volcanic eruptions, IV. The control of magma properties and conduit geometry on eruption column behavior. Geophys. J. R. Astron. Soc., 63: 117–148.